Modeling Study of Ice Formation in Warm-Based Precipitating Shallow Cumulus Clouds

JIMING SUN

Laboratory of Cloud-Precipitation Physics and Severe Storms (LACS), Institute of Atmospheric Physics, Chinese Academy of Sciences, Beijing, China, and Department of Atmospheric and Oceanic Sciences, McGill University, Montreal, Quebec, Canada

PARISA A. ARIYA

Department of Atmospheric and Oceanic Sciences, and Department of Chemistry, McGill University, Montreal, Quebec, Canada

HENRY G. LEIGHTON AND MAN KONG YAU

Department of Atmospheric and Oceanic Sciences, McGill University, Montreal, Quebec, Canada

ABSTRACT

Observations of large concentrations of ice particles in the dissipating stage of warm-based precipitating shallow cumulus clouds point to the limitations of scientists' understanding of the physics of such clouds and the possible role of cloud dynamics. The most commonly accepted mechanisms of ice splinter production in the riming process have limitations to properly explain the rapid production of ice bursts. A more detailed description of the temporal and spatial evolution of hydrometeors and their interaction with cloud condensation nuclei and ice nuclei is needed to understand this phenomenon. A cloud model with bin-resolved microphysics can describe the time-dependent evolution of liquid droplets and ice particles and provide insights into how the physics and dynamics and their interaction may result in ice initiation and ice multiplication. The authors developed a 1.5-dimensional non-hydrostatic convective cloud and aerosol interaction model with spectral (bin) microphysics. The number and mass concentrations of aerosols, including ice nuclei and cloud condensation nuclei, were explicitly followed. Since both in situ observations of bioaerosols and laboratory experiments pointed to efficient nucleation capabilities at relative warm temperatures, it was assumed that ice-nucleating bioaerosols are involved in primary ice particle formation in condensation and immersion modes. Results show that bioaerosols can be the source of primary ice pellets, which in turn lead to high ice concentrations.

1. Introduction

Ice formation in both deep and shallow cumulus clouds impacts the atmospheric circulation through its impact on precipitation, on diabatic heating, and on the earth's radiation budget because of the differences of the optical properties of water and ice particles. Although shallow cumulus clouds are widespread in the tropics and subtropics (Rangno and Hobbs 2005; Masunaga and Kummerow 2006; Warren et al. 2007), the ice formation mechanism in warm-based precipitating shallow cumulus clouds (WPSCCs) is not well understood (Rangno and Hobbs 2005).

The rapid formation of exceptionally high ice particle concentrations in WPSCCs has often been observed in both maritime and continental regions (Koenig 1963; Mossop 1968; Hobbs and Rangno 1998; Baker 2001). However, concentrations of ice nuclei (IN) in the atmosphere that are active at relatively warm temperatures are very low (Mohler et al. 2007). Mechanisms

Corresponding author address: Jiming Sun, Laboratory of Cloud-Precipitation Physics and Severe Storms (LACS), Institute of Atmospheric Physics, Chinese Academy of Sciences, Beijing 100029, China.
E-mail: jimings@mail.iap.ac.cn

other than primary ice formation must play an important role in the ice formation of a WPSCC (Rangno and Hobbs 2005). To elucidate ice multiplication in WPSCCs, we should resolve two related scientific issues: 1) the evolution of cloud droplet spectra in cumulus clouds and 2) the possible candidates for IN and ice nucleation mechanisms triggered by them in WPSCCs.

Ice formation in WPSCCs is strongly related to their cloud droplet spectra (Hobbs and Rangno 1998). Observations show that cumulus cloud droplet spectra are broader than those predicted by condensational growth in an adiabatically ascending parcel that is only driven by buoyancy. However, both buoyancy and pressure perturbations determine the development of cumulus clouds (List and Lozowski 1970; Yau 1979; Schlesinger 1980; Zhao and Austin 2005). Therefore, it is necessary to simulate the impact of pressure perturbations on the droplet spectral evolution in cumulus clouds. Sun et al. (2010) found that the cloud droplet spectrum evolution of WPSCCs is favorable for ice multiplication through the Hallett–Mossop (H–M) mechanism in the simulations with perturbation pressures considered. However, little is known about the candidates of IN and ice nucleation mechanisms in WPSCCs. Even though Ariya et al. (2009) proposed that ice-nucleating bioaerosols may act as IN to trigger the ice multiplication in WPSCCs, there is much we still do not know about the minimum concentration of bioaerosols and the prevalent nucleation mode required to trigger ice multiplication in WPSCCs. Condensation freezing may play an important role in the primary ice formation of WPSCCs in addition to immersion freezing, which is considered only as an nucleation mode in the simulations for such clouds (Ariya et al. 2009; Sun et al. 2010). The sources and chemical compositions of IN in the atmosphere have been a puzzling issue for several decades, and there is still much to be learned in this area. Evidence keeps emerging in favor of both mineral and carbonaceous origins of ice nuclei. In situ observations further showed that biological particles dominate the carbonaceous fraction in some regions (Pratt et al. 2009; Prenni et al. 2009). Soil dust and biological particles are the predominant IN active at relatively warm temperatures (Phillips et al. 2009; Pratt et al. 2009).

The main components of mineral dusts have different ice-forming capabilities. The temperatures at which ice starts to be nucleated by silicate particles range between $-10°$ and $-20°C$, and other particles, such as kaolinite and montmorillonite, have an ice initiation temperature as cold as $-35°C$ via the deposition mode when ice supersaturation is greater than 10% (Welti et al. 2009).

Connolly et al. (2009) found that mineral dusts from Asia, the Sahara Desert, and Arizona are not active as IN at temperatures warmer than $-12°C$. In recent years, airborne IN observed in the atmosphere have been mainly associated with mineral dusts (DeMott et al. 2003; Richardson et al. 2007; Klein et al. 2010; Chou et al. 2011). However, using an atmospheric lidar, Ansmann et al. (2008) suggested that dust aerosols may not be effective as IN at temperatures warmer than $-18°C$, since ice particles at warmer temperatures were not found at the top of altocumulus clouds at locations close to the Sahara. Even though a recent observation showed that Saharan dust aerosols transported to central Europe can initiate ice particles at temperatures as warm as $-8°C$ (Klein et al. 2010), mineral particles may only be partial contributors and not the dominant sources of atmospheric IN at relatively warm temperatures (warmer than $-10°C$). Biological particles have been identified as a widespread source of IN in almost all climates (Szyrmer and Zawadzki 1997; Sun 2008) in both continental regions (Pratt et al. 2009; Prenni et al. 2009) and oceanic regions (Knopf et al. 2011). Bioaerosols collected in precipitation show high nucleation capacities at relatively warm temperatures (Christner et al. 2008). Bowers et al. (2009, 2010) further found airborne bacteria acting as IN at temperatures above $-10°C$. The ubiquity and the high ice-nucleating ability of bioaerosols may render them as an important player in cloud ice formation at relatively warm temperatures. DeMott and Prenni (2010) suggested that carbonaceous aerosols acting as IN in clouds warmer than $-15°C$ are likely to be airborne biological particles. Note that there is a large variety of biological particle concentrations (Burrows et al. 2009). We still do not know the potential roles for biological particles in atmospheric processes (Morris et al. 2011). Recent studies found that biological ice nucleus concentrations are not important on the global scale in cloud formation (Hoose et al. 2010a; Sesartic et al. 2011). However, their roles in atmospheric processes may be important on a small scale and at warm temperatures.

Considering the direct and indirect evidence described above, we suggest that likely candidates for efficient IN at warm temperatures in the atmosphere might be bioaerosols and that they might be expected to play an important role in ice crystal formation in WPSCCs. However, little is known about ice initiation mechanisms of ice-nucleating bioaerosols in WPSCCs and the relationship between huge concentrations of ice particles in WPSCCs (Rangno and Hobbs 2005) and the low concentrations of biological IN in the atmosphere (Hoose et al. 2010b,a).

To accomplish this, it is necessary to numerically simulate how the ice nucleation by ice-nucleating bioaerosols occurs in WPSCCs microphysically and dynamically. Diehl and Wurzler (2010) used an air parcel model to simulate ice nucleation by bacteria with bin microphysics. Phillips et al. (2009) investigated the role of bioaerosols in ice formation with bulk microphysics. Parcel models are dynamically too simple to describe the cloud droplet spectrum evolution of cumulus clouds because the most important property of the air continuity cannot be considered in such models. Furthermore, bulk microphysics cannot microphysically describe the evolution of the IN-containing cloud droplet spectra properly. To overcome these problems within current computation limitations, we use a two-cylinder time-dependent cloud and aerosol interaction model that incorporates explicit microphysical processes for cloud condensation nuclei (CCN) and IN. Section 2 provides the dynamical framework of the model. Section 3 describes microphysical processes of the model. Section 4 presents the model setup. Section 5 describes simulations based on a parameterization that is constrained by observations. Section 6 presents a sensitivity study of the effects of aerosol concentrations on ice formation in WPSCCs. Section 7 presents results based on a parameterization constrained by results from laboratory experiments.

2. Dynamical framework

To study ice nucleation and ice multiplication, not only is high resolution of the particle size bins necessary to adequately describe the distributions of aerosol particles (CCN and IN) and water droplets and ice particles, but also the mass of CCN or IN in hydrometeors should be followed. Since such requirements need an explicit treatment of the hygroscopic growth of aerosols from the nanometer size range of dry aerosols to the millimeter size range of hydrometeors, we had to choose a 1.5-dimensional (1.5D) Eulerian model due to the current limited computational resources. The model described here has been used to simulate ice formation in WPSCCs (Ariya et al. 2009; Sun et al. 2010). The more detailed description is needed to clarify the advantages and the disadvantages of this model. The first 1.5D cylindrical model was presented by Asai and Kasahara (1967) to investigate the influence of the compensating downward motions on cumulus cloud formation and evolution. In such a model, two circular concentric air columns describe the updraft/cloud region (inside column) and the compensating downward-motion region (outside column). A 1.5D model allows us to describe the exchange processes between the lateral sides of the two cylinders. Holton (1973) further developed a parameterization method to include perturbation pressure in a 1D model. Yau (1980) presented a method to include explicit computation of perturbation pressure. Including perturbation pressure resolved the modeling problem of unrealistically large gradients of vertical velocities at the tops of simulated cumulus clouds. We further assume that horizontally, the vertical wind velocities are distributed sinusoidally in order to allow for a vortexlike circulation at the cloud top (Zhao and Austin 2005). Vertical eddy fluxes were also calculated in order to consider the changes of the vertical distribution of heat, momentum, aerosols, and hydrometeors induced by wind velocity deformation and thermal instability. The ratio of the horizontal size of the updraft region and that of the compensating downward-motion region impacts the evolution of the simulated cumulus clouds (Yau 1980). The radii ratio of the two cylinders has been specified to be 0.16 (Ariya et al. 2009; Sun et al. 2010). We performed many sensitivity tests and compared model runs with observations of the Cooperative Convective Precipitation Experiment (CCOPE) case (19 July 1981) (Dye et al. 1986). The radii ratio of 0.25 can result in a good agreement between the observations and the simulations.

The dynamics of this model are shown in Fig. 1a. Lateral exchanges between the two cylinders are allowed through the horizontal velocity $\tilde{u}$. The vertical wind velocities w_a and w_b are horizontally distributed sinusoidally. The equations in the inner cylinder are written as follows:

a. Vertical motions

$$\frac{\partial(\rho_0 \overline{w}_a)}{\partial t} = -\frac{\partial(\overline{w}_a \rho_0 \overline{w}_a)}{\partial z} - \frac{2}{a}\rho_0 \tilde{w}_a \tilde{u}_a + \frac{2}{a}\alpha^2 \rho_0 |\overline{w}_b - \overline{w}_a|(\overline{w}_b - \overline{w}_a) - \rho_0 \frac{\partial\left(K_M \frac{\partial \overline{w}_a}{\partial z}\right)}{\partial z}$$

$$- c_p \theta_0 \rho_0 \frac{\partial \overline{\pi}' a}{\partial z} + \left[\frac{\overline{\theta}_{va} - \overline{\theta}_{vab}}{\overline{\theta}_{vab}} - (\overline{q}_{ca} + \overline{q}_{ia})\right]\rho_0 g \qquad (1)$$

b. Thermodynamic equation

$$\frac{\partial(\rho_0\overline{\theta}_a)}{\partial t} = -\frac{\partial(\overline{w}_a\rho_0\overline{\theta}_a)}{\partial z} - \frac{2}{a}\rho_0\tilde{\theta}_a\tilde{u}_a$$
$$+ \frac{2}{a}\alpha^2\rho_0|\overline{w}_b - \overline{w}_a|(\overline{\theta}_b - \overline{\theta}_a)$$
$$- \rho_0\frac{\partial\left(K_H\dfrac{\partial\overline{\theta}_a}{\partial z}\right)}{\partial z} + \frac{L\theta_0}{c_p T_0}\frac{\partial\rho_0\overline{q}_{va}}{\partial t}\bigg|_{\text{mic}} \quad (2)$$

c. Continuity of water vapor

$$\frac{\partial(\rho_0\overline{q}_{va})}{\partial t} = -\frac{\partial(\overline{w}_a\rho_0\overline{q}_{va})}{\partial z} - \frac{2}{a}\rho_0\tilde{q}_{va}\tilde{u}_a$$
$$+ \frac{2}{a}\alpha^2\rho_0|\overline{w}_b - \overline{w}_a|(\overline{q}_{vb} - \overline{q}_{va})$$
$$- \rho_0\frac{\partial\left(K_M\dfrac{\partial\overline{q}_{va}}{\partial z}\right)}{\partial z} + \frac{\partial\rho_0\overline{q}_{va}}{\partial t}\bigg|_{\text{mic}} \quad (3)$$

d. Continuity of hydrometeors

$$\frac{\partial\overline{f}_{\text{wat/ice},a}}{\partial t} = -\frac{\partial(\overline{w}_a - U_{\infty,\text{wat/ice}})\overline{f}_{\text{wat/ice},a}}{\partial z} - \frac{2}{a}\tilde{f}_{\text{wat/ice},a}\tilde{u}_a$$
$$+ \frac{2}{a}\alpha^2|\overline{w}_b - \overline{w}_a|(\overline{f}_{\text{wat/ice},b} - \overline{f}_{\text{wat/ice},a})$$
$$- \frac{\partial\left(K_M\dfrac{\partial\overline{f}_{\text{wat/ice},a}}{\partial z}\right)}{\partial z} + \frac{\partial\overline{f}_{\text{wat/ice},a}}{\partial t}\bigg|_{\text{mic}}, \quad (4)$$

where a is the inside radius, b is the outside radius, the ratio of a and b is 0.25, we assumed that a is 1.5 km for warm-based shallow convection, variables with the subscript a represent variables of the inner cylinder, variables with the subscript b represent variables between the inner cylinder and outer cylinder, α^2 is set to 0.1 (Asai and Kasahara 1967), and $f_{\text{wat/ice}}$ denotes the number density distribution function of water droplets or ice crystals. Also, w denotes the vertical velocity, $U_{\infty,\text{wat/ice}}$ is the terminal velocity of hydrometeors, θ is the potential temperature, θ_v is the virtual potential temperature, and q_v is the mixing ratio of water vapor. The bar above a symbol denotes the average values over the inner cylinder domain and over a domain between the inner cylinder and the outer cylinder. The variables with a tilde represent the effect of dynamic entrainment. The variable π' denotes the deviation of nondimensional pressure from the basic state; ρ_0 and θ_0 are the base-state air density and

potential temperature for a hydrostatic atmosphere, respectively; T_0 is the base-state temperature; c_p is the specific heat of dry air at constant pressure; g is the acceleration of gravity; L is the specific latent heat released in phase changes; and K_M and K_H represent the eddy viscosity coefficients of momentum and heat, respectively.

In the above equations on the right-hand side, the first term represents the vertical flux divergence; the second term represents the lateral exchanges, in which horizontal advection can be performed; the third term is the lateral eddy flux; and the fourth term is the vertical subgrid eddy flux. In Eq. (1), the fifth term represents the vertical pressure gradient force of the nondimensional pressure perturbation and sixth term is the buoyancy force. In Eqs. (2)–(4), the fifth term represents the variable changes due to microphysical processes. The explicit solutions of the perturbation pressure and the vertical eddy fluxes are described by Sun (2008).

3. Microphysical processes

The microphysical processes of this model especially focus on the interactions between aerosols and clouds. The properties of the atmospheric aerosol are much more complicated than can be described faithfully in cloud models. It is plausible that a considerable portion of aerosols in the atmosphere are suitable candidates for CCN. IN that are active at temperatures warmer than $-35°C$, however, can only come from a very small fraction of those aerosols that contain insoluble substances. It is impossible to track the proportions of CCN and IN in each hydrometeor. Instead, we define two functions, $f(m, m_{\text{ap}})$ and $g(m, m_{\text{IN}})$. The former is the concentration of hydrometeors (either water or ice) of mass m that contain any particle (solid or dissolved) (e.g., ammonium sulfate and/or IN) of mass m_{ap}; for most hydrometeors m_{ap} will be the CCN mass. The latter is the concentration of hydrometeors of m that contains an ice nucleus of mass m_{IN}, regardless of the total particle mass in the hydrometeor. So, $g(m, m_{\text{IN}})$ is a subset of $f(m, m_{\text{ap}})$. The meaning of functions used in our model with a fixed-bin scheme is described in Table 1.

In this model, the sizes of cloud droplets growing from haze droplets and raindrops growing via the warm-rain process are determined by condensation, evaporation, and stochastic collision and coalescence (Leroy et al. 2006; Sun 2008). The ice-phase microphysics includes nucleation, deposition, sublimation, aggregation, riming, and melting. Since we focus on ice nucleation and ice multiplication, ice particles are characterized as small spherical ice particles, including frozen cloud droplets (diameters less than 20 μm) and newly produced spherical ice splinters (Choularton et al. 1978),

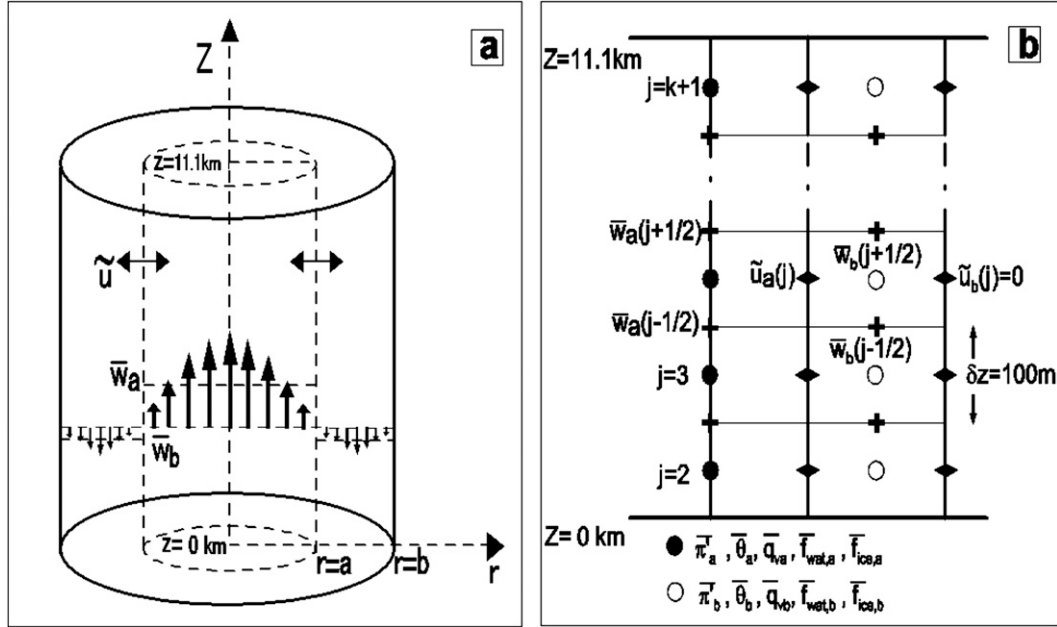FIG. 1. (a) Schematic view of the cloud (radius a; $a = 3.0$ km for deep convection, $a = 1.5$ km for shallow convection) and subsidence (radius $b - a$; $b = 12.0$ km for deep convection, $b = 6.0$ km for shallow convection) columns for a 1.5D model. (b) The vertically staggered grid of two cylinders showing full levels and half levels.

with an assumed lognormal size distribution (standard deviation σ is 1.15; the mean radius r_m is 5.0 μm); columnar ice particles (see Hobbs and Rangno 1990, their Fig. 6) (diameters from 20 to 100 μm of size bins); and spherical ice particles [see Hobbs and Rangno (1990), their Fig. 6] (diameters from 100 to 600 μm of size bins). For the size bins of ice particles between 600 and 5000 μm, ice pellets have been implemented into the model for the simulations of WPSCCs. The ice spectrum of these shapes and types is presented by a 1D spectral function in our model. The density of ice particles has been assumed to be 0.9 cm^{-3}. With these prescribed characteristics, the diffusional and rime growth rates of ice particles with different shapes can be used to determine the ice particle mass increase as a spherical body with a normalized bulk density of 1.0 g cm^{-3} in each size bin. In the size range of columnar ice particles (20–100 μm), the axis ratio is assumed to change sinusoidally with the mass increase to keep the spectral distribution of ice particles continuous, with a maximum ratio of 10.

a. Microphysical processes for CCN

The hygroscopic growth of CCN is described as a continuous process through which haze drops become activated to form cloud drops. In this study, we further assume that CCN are predominantly composed of ammonium

sulfate and that the impurity effect on cloud droplet activation (Sun and Ariya 2006) is ignored if aerosols contain other soluble or insoluble substances. Cloud droplets grow by condensation and collision–coalescence; meanwhile, some supercooled water droplets can also transform into ice particles. Water droplets can freeze in three ways in our model: the nucleation of cloud and rain droplets by IN, the freezing of rain droplets by collision with ice splinters, and the collision of haze droplets and cloud droplets with ice particles with equivalent spherical water droplet diameters greater than 100 μm (riming process). The whole process for the evolution of the water droplet and ice particle distributions (appendix A) is described in Eqs. (5) and (6), respectively:

TABLE 1. Number distribution functions used in the 1.5D model.

Functions	Total bins of aerosols	Total bins of hydrometeors
$f_{water}(m, m_{ap})$	90 mass bins of ammonium sulfate	130 mass bins of water drops
$f_{ice}(m, m_{ap})$	90 mass bins of ammonium sulfate	130 mass bins of ice particles
$g_{water}(m, m_{IN})$	90 mass bins of ice nuclei	130 mass bins of water drops
$g_{ice}(m, m_{IN})$	90 mass bins of ice nuclei	130 mass bins of ice particles

$$\left.\frac{\partial f_{\text{wat}}(m, m_{\text{ap}})}{\partial t}\right|_{\text{mic}} = \left.\frac{\partial f_{\text{wat}}}{\partial t}\right|_{\text{condensation/evaporation}}$$

$$- \left.\frac{\partial f_{\text{ice}}}{\partial t}\right|_{\text{nucleation}} - \left.\frac{\partial f_{\text{wat}}}{\partial t}\right|_{\text{riming}}$$

$$+ \left.\frac{\partial f_{\text{wat}}}{\partial t}\right|_{\text{coalescence}} + \left.\frac{\partial f_{\text{wat}}}{\partial t}\right|_{\text{melting}}, \tag{5}$$

$$\left.\frac{\partial f_{\text{ice}}(m, m_{\text{ap}})}{\partial t}\right|_{\text{mic}} = \left.\frac{\partial f_{\text{ice}}}{\partial t}\right|_{\text{deposition/sublimation}}$$

$$+ \left.\frac{\partial f_{\text{ice}}}{\partial t}\right|_{\text{nucleation}} + \left.\frac{\partial f_{\text{ice}}}{\partial t}\right|_{\text{riming}}$$

$$+ \left.\frac{\partial f_{\text{ice}}}{\partial t}\right|_{\text{aggregation}} - \left.\frac{\partial f_{\text{ice}}}{\partial t}\right|_{\text{melting}}. \tag{6}$$

b. Microphysical processes for IN

Heterogeneous freezing of ice in laboratory experiments can occur in association with IN, via condensation, immersion, deposition, and contact mechanisms. It is not feasible to include all these nucleation mechanisms in our simulations. Since only a small fraction of aerosols in the atmosphere are IN and their aged surfaces are always covered with soluble substances (Chen et al. 1998; Zhang and Carmichael 1999; Clarke et al. 2004; Sun and Ariya 2006; Pratt et al. 2010) and heterogeneous ice nucleation rarely occurred below water saturation (Heymsfield and Miloshevich 1993; Mohler et al. 2005; Dymarska et al. 2006), we consider that IN catalyzing ice formation through immersion freezing and condensation freezing are a part of the CCN distribution and are only distinguished from CCN by their extra property of nucleating ice as defined in the function of $g(m, m_{\text{IN}})$. We further assume that IN are composed of a single kind of particle with soluble material on its surface. There are two ways that hydrometeors can contain IN in our model: one way is that IN become activated as cloud droplets and another way is that IN are captured by hydrometeors by Brownian motion and by hydrodynamic capture (Sun 2008). To follow the distribution of particles that contain IN, we have the following equations that are equivalent to those for the whole hydrometeor distribution:

$$\left.\frac{\partial g_{\text{wat}}(m, m_{\text{IN}})}{\partial t}\right|_{\text{mic}} = \left.\frac{\partial g_{\text{wat}}}{\partial t}\right|_{\text{condensation/evaporation}}$$

$$- \left.\frac{\partial g_{\text{ice}}}{\partial t}\right|_{\text{ice nucleation}} - \left.\frac{\partial g_{\text{wat}}}{\partial t}\right|_{\text{riming}}$$

$$+ \left.\frac{\partial g_{\text{wat}}}{\partial t}\right|_{\text{coalescence}} + \left.\frac{\partial g_{\text{wat}}}{\partial t}\right|_{\text{melting}}, \tag{7}$$

$$\left.\frac{\partial g_{\text{ice}}(m, m_{\text{IN}})}{\partial t}\right|_{\text{mic}} = \left.\frac{\partial g_{\text{ice}}}{\partial t}\right|_{\text{deposition/sublimation}}$$

$$+ \left.\frac{\partial g_{\text{ice}}}{\partial t}\right|_{\text{ice nucleation}} + \left.\frac{\partial g_{\text{ice}}}{\partial t}\right|_{\text{riming}}$$

$$+ \left.\frac{\partial g_{\text{ice}}}{\partial t}\right|_{\text{aggregation}} - \left.\frac{\partial g_{\text{ice}}}{\partial t}\right|_{\text{melting}}. \tag{8}$$

The detailed description of the above expressions can be found in appendix B.

c. Parameterizations of heterogeneous ice nucleation and ice multiplication

We selected two specific parameterizations of heterogeneous ice nucleation for ice formation comparisons in WPSCCs. One parameterization that provides dependencies on the chemistry and surface area of IN has an observational constraint (Phillips et al. 2008). The second is based on laboratory observations (Diehl and Wurzler 2004).

1) OBSERVATIONAL CONSTRAINT PARAMETERIZATION

Phillips et al. (2008) proposed an empirical parameterization of heterogeneous ice nucleation through deposition, condensation, and immersion freezing for dust/metallic aerosols (DM), inorganic black carbon (BC), and insoluble organic particles (O) in which bacteria are assumed to be the ice-nucleating material. The number of active IN per kilogram of air for each kind of aerosol $n_{\text{IN},X}$ is determined by air temperature, supersaturation with respect to ice, nucleation threshold temperature, fractional contribution of this kind of IN to the measured total IN concentrations, concentrations, and size distributions of a particular species of insoluble aerosol. A detailed description of the parameterization is given by Phillips et al. (2008). In our simulations, we only consider ice nucleation at water supersaturation.

2) LABORATORY-BASED PARAMETERIZATION

The immersion freezing mode is one ice initiation mechanism that is relevant to this study. We simulated ice nucleation in the immersion freezing mode with the parameterization of Diehl and Wurzler (2004). The immersion freezing rate of IN is based on the semiempirical method, defined as

$$R(m, m_{\text{IN}}) = -a B_{h,i} V_{\text{drop}} \exp[a(T_0 - T)]\frac{dT}{dt}, \tag{9}$$

where a is equal to 0.82 °C^{-1}; V_{drop} is the volume of the water droplet; T_0 is equal to 273.16 K; $B_{h,i}$ is a constant

representing the ice-nucleating capability of IN, which relates the median freezing temperature T_m (Diehl and Wurzler 2004) and the volume of the drops V_{drop} (Pruppacher and Klett 1997); and dT/dt is the rate of temperature change of the cloud parcel. The temperature changes of saturated air parcels follow the modified pseudomoist adiabat (Taylor 1989).

d. Ice multiplication

Laboratory experiments have documented the dependence of secondary ice production rates on temperature, the water drop spectrum, and riming rate (Mossop 1976, 1978b,a; Heymsfield and Mossop 1984), and the results have been expressed mathematically in various ways (Mossop 1978b; Harris-Hobbs and Cooper 1987; Cardwell et al. 2003). We have implemented the parameterization of secondary ice production of Harris-Hobbs and Cooper (1987) in the present model (see appendix C).

4. Model setup

a. Finite-difference scheme

The numerical transport algorithm adopted is the Multidimensional Positive Definite Advection Transport Algorithm (MPDATA) with the nonoscillatory option (Smolarkiewicz and Grabowski 1990; Schär and Smolarkiewicz 1996). Our model employs second-order-accurate MPDATA for both momentum and scalar variables involved in the dynamics and microphysics of hydrometeor growth. The number density distribution of aerosol particles, water droplets (including aerosol particles), and ice crystals are described by two number density distribution functions—$f_{water}(\ln m)$ and $f_{ice}(\ln m)$—with respect to the natural logarithm of mass (Leroy et al. 2006). Aerosol particles have 90 bins with a radius from 8.0×10^{-3} to 2.36×10^{2} μm, and hydrometeors and aerosols together have 130 bins with a radius from 8.0×10^{-3} to 2.4×10^{4} μm, so that the minimum mass of aerosols m_{ap0} is 2.0×10^{-18} g.

The time step is 2 s, and a time-splitting procedure is applied in the numerical transport algorithm for both dynamical processes and microphysical processes in order to guarantee the Courant–Friedrich–Levy criterion.

b. Initial conditions

The initial thermodynamic conditions for the simulations of WPSCCs are the same as those used by Yau (1980) to represent an idealized sounding to simulate cumulus clouds. The temperatures at the sea surface and at the cloud base (800 m) are 24° and 17°C, respectively.
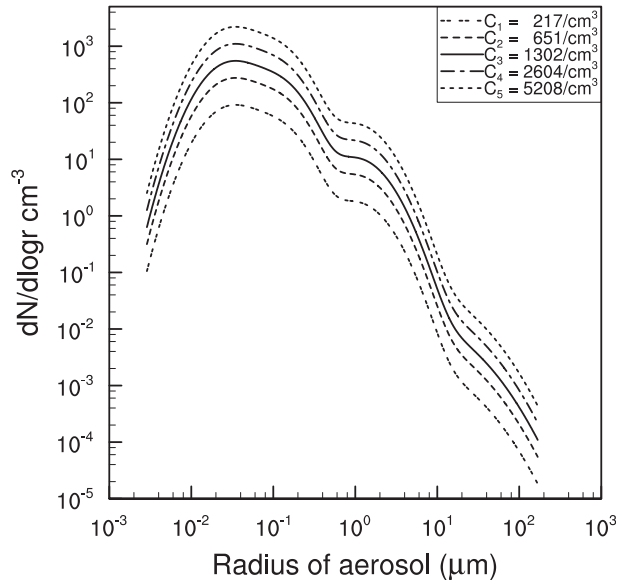

FIG. 2. Typical maritime aerosol distribution and multiplied aerosol distributions for simulations.

The ambient temperature lapse rate is 6°C km^{-1} above the cloud base. To initiate convection we use a perturbation of vertical velocity. The initial vertical velocity impulse below cloud base is assumed to be

$$w'_a = \sin\left(\frac{\pi z}{H}\right), \quad z \leq H, \tag{10}$$

where H is the height of the cloud base.

Figure 2 shows the size distribution of maritime aerosols (O'Dowd et al. 1997) together with multiples of the distributions. The concentration of maritime aerosol C_1 represents a clean ocean region; the threefold increase in the maritime aerosol concentration C_2 represents a clean continental region; the sixfold increase in the maritime aerosol concentration C_3 represents a slightly polluted continental environment; the twelvefold increase in the maritime aerosol concentration C_4 represents a medium-polluted continental region; and the twenty-fourfold increase in the maritime aerosol concentration C_5 represents a heavily polluted continental region as may, for example, be found in response to biomass burning (Jayaratne and Verma 2001). A 6-times maritime aerosol concentration (C_3) is used as the control case study. The initial aerosol concentrations in all cases decreased exponentially with height above cloud base. Aerosols with diameters greater than 10 μm are not included in the simulations. The initial size of drops is determined by classical Kohler theory. The maximum size of haze drops is calculated by assuming equilibrium at 99% relative humidity at the cloud base.

5. Simulations based on the parameterization constrained by observations

In the parameterization scheme of Phillips et al. (2008), IN are dust particles, soot/black carbon, and bio-aerosols represented by bacteria. The proportional contribution of each aerosol type to IN has been assumed to have a constant value that is independent of temperature and humidity. The relative contributions of dust and soot were set at $2/3$ and $1/3 - 0.06$ [see Phillips et al. (2008), their Fig. 2], respectively. The estimate of the bacterial fraction, 0.06, was derived from the comparison of the total IN concentration predicted by the parameterization of Meyers et al. (1992) at $-30°C$ with the bacterial IN concentration that was estimated with a given concentration of bacterial cells, the fraction of the ice-nucleating bacteria of 1% (Lindemann et al. 1982), and the freezing fraction of cells belonging to the ice-nucleating bacteria of 0.1 at the same temperature (Vali et al. 1976; Gross et al. 1983).

Since we focus on the study of ice initiation and ice multiplication in WPSCCs in which cloud-top temperatures are around $-10°C$, the concentration of IN at $-10°C$ in the atmosphere should be the upper bound on the ice nucleus concentrations and hence ice initiation at temperatures warmer than $-10°C$. The concentration of IN active at temperatures warmer than $-10°C$ is normally less than $0.3 L^{-1}$ [see Eidhammer et al. (2009), their Fig. 7]. Berezinski et al. (1988) observed an IN concentration of $0.27 L^{-1}$ at $-10°C$. Therefore, we assumed that the initial concentrations of bioaerosols, including non-ice-nucleating bioaerosols, are equal to different multiples of the concentration of IN at $-10°C$, which vary in the in situ observation range (Burrows et al. 2009; Després et al. 2012). Furthermore, the impacts of concentrations of ammonium sulfate on ice formation should be also evaluated, since the size distribution and concentrations of cloud droplets impact the ice multiplication. Therefore, experiments listed in Table 2 include tests for concentrations of bacteria and concentrations of ammonium sulfate. We used the experiment E_4 as a control run for our study.

Note that both the initial size distribution of IN and their hygroscopicity influence their collision efficiencies with hydrometeors. The size distribution (Tong and Lightart 2000) and the activation of bacteria as CCN (Franc and DeMott 1998) are taken into account in our study. The size distribution of IN is selected to be a combination of two measured bacterial lognormal size distributions (Qian et al. 1995; Tong and Lightart 2000): for single cells, σ is 1.35 and r_m is 0.78 μm; for clusters, $\sigma = 1.35$ and $r_m = 1.97$ μm. This size distribution of bacteria results in the minimum bacterial mass m_{IN0} to be

TABLE 2. Experimental simulations.

Case	Total concentration of aerosols	Concentration of bacteria (L^{-1})
E_1	C_3	0.27
E_2	C_3	5×0.27
E_3	C_3	25×0.27
E_4	C_3	50×0.27
E_5	C_3	100×0.27
E_6	C_1	50×0.27
E_7	C_2	50×0.27
E_8	C_4	50×0.27
E_9	C_5	50×0.27

2.048×10^{-15} g. The concentrations of single-cell particles and cluster-cell particles occupy 40% and 60% of the total bacterial particles, respectively.

a. Time evolution of selected variables

The time evolution of vertical velocities and rainwater contents are shown in Fig. 3a. A significant feature of the results is the weak vertical gradient of vertical velocity compared with other studies using a similar dynamical framework (Asai and Kasahara 1967; Taylor 1989; Leroy et al. 2006). The strong gradient of vertical velocity found in previous studies resulted from inadequate treatment of the pressure perturbation (Sun 2008). In this study, we took account of the impact of rotation of the airflow on the perturbation pressure with an assumption that horizontal and vertical velocities are distributed sinusoidally. Furthermore, the gradient force of dynamic perturbation pressure (perturbation pressure induced by dynamic field) leads to acceleration at the cloud top and may speed up warm-rain formation (Sun 2008). A rainwater content greater than $0.1 g m^{-3}$ appears within 35 min after the convection initiation with a multiplied maritime aerosol concentration ($6 \times 217 cm^{-3}$) (Fig. 3a). Liquid water converts into ice water in the cloud dissipating stage (Fig. 3b). The maximum ice water content reaches $0.5 m^{-3}$. Figure 4 shows the spatial and temporal evolution of water drop concentrations. The maximum cloud droplet concentration reaches $600 cm^{-3}$ (Fig. 4a). At the top of the cloud, there is a high concentration band of small raindrops (Fig. 4a). Correspondingly, the maximum concentration of bacteria-containing cloud droplets is $0.0025 cm^{-3}$ (Fig. 4b). The spatial and temporal distribution of bacteria-containing raindrop concentrations is almost the same as that of the total raindrop concentrations, which means that all raindrops with a diameter greater than 2 mm contain bacteria. Bacteria are scavenged by raindrops through both nucleation and impaction scavenging. However, the maximum concentration of bacteria-containing small raindrops is less than that of total
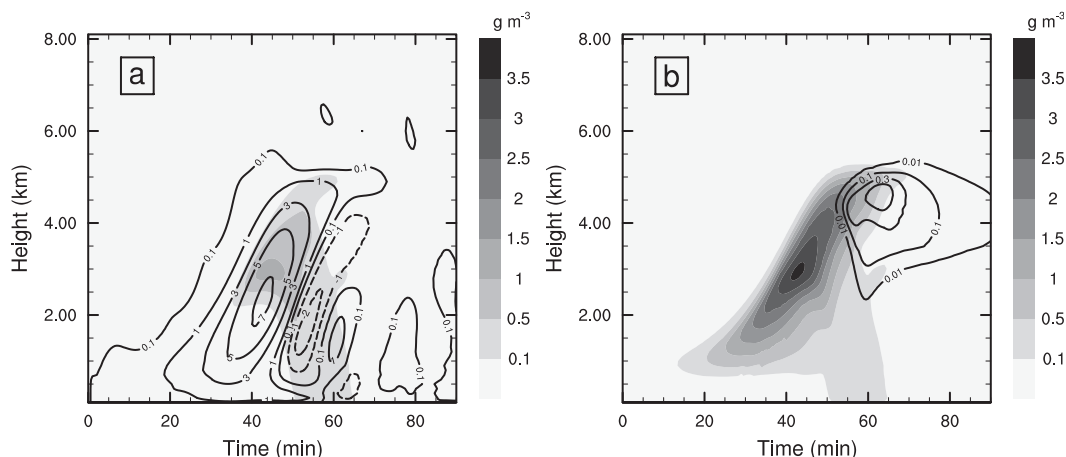
FIG. 3. Spatial and temporal evolution of vertical velocity and liquid and ice water content in the inner cylinder for the case E$_4$. (a) Vertical velocity (m s^{-1}, solid and dashed lines) and rainwater content (drop diameters > 100 μm) (g m^{-3}, shaded area). (b) Liquid water content (g m^{-3}, shaded area) and ice water content (g m^{-3}, solid lines).

small raindrops during most time periods. Therefore, some small raindrops do not contain bacteria in this simulation with an initial bacterial concentration of 13.5 L^{-1} in which the concentration of ice-nucleating bacteria is 0.135 L^{-1}. Figure 5 shows the primary ice nucleation rate and the ice splinter production rate. The primary ice nucleation occurs both at the cloud-top interface of cloud-clear air through the condensation freezing mode and in the cloud through the immersion freezing mode. The maximum primary ice nucleation rate (MPINR) only reaches 1.038×10^{-3} L^{-1} s^{-1}. However, the maximum ice splinter production rate (MISPR) reaches 1.206 L^{-1} s^{-1}. These results indicate that the ice multiplication dominates ice formation in WPSCCs.

In the subfreezing region, the maximum concentration of ice particles containing bacteria reaches 1.0 L^{-1} in the dissipating stage (Fig. 6a). Bacteria-containing ice particles include bacteria-containing primary ice particles and bacteria-containing secondary ice particles. Bacteria-containing primary ice particles refer to ice particles nucleated by ice-nucleating bacteria and subsequent rimed ice particles resulting from collisions with cloud droplets and raindrops. Bacteria-containing secondary ice particles refer to ice particles nucleated by ice splinters that subsequently rimed with bacteria-containing water drops. Since in the parameterization scheme of Phillips et al. (2008) bacteria include ice-nucleating bacteria and nonice-nucleating bacteria, IN-containing ice particles refer to
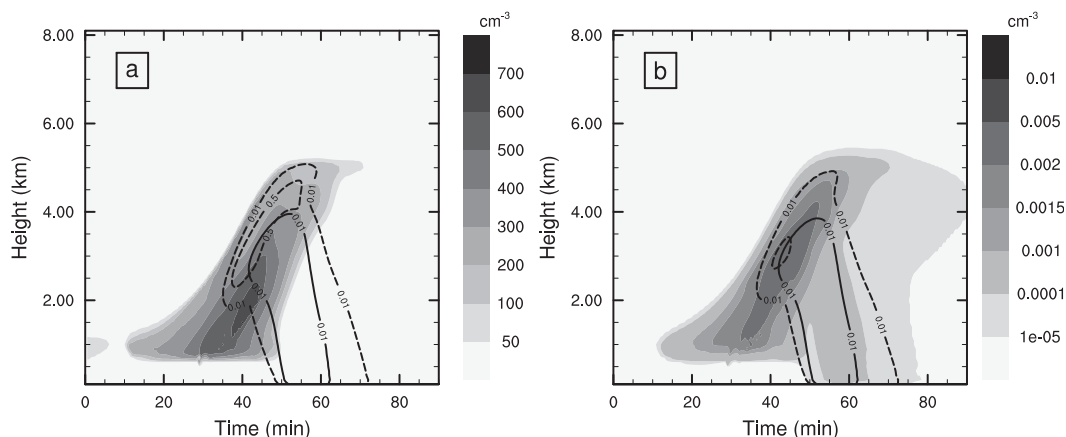

FIG. 4. Spatial and temporal evolution of water drop concentrations in different size categories in the inner cylinder for the case E$_4$. (a) Cloud drops with diameters > 1.0 μm (cm^{-3}, shaded area), small raindrops with diameters > 600 μm (L^{-1}, dashed lines), and raindrops with diameters > 2 mm (L^{-1}, solid lines). (b) Bacteria-containing cloud droplets with diameters > 1.0 μm (cm^{-3}, shaded area), bacteria-containing small raindrops with diameters > 600 μm (L^{-1}, dashed lines), and bacteria-containing raindrops with diameters > 2 mm (L^{-1}, solid lines).
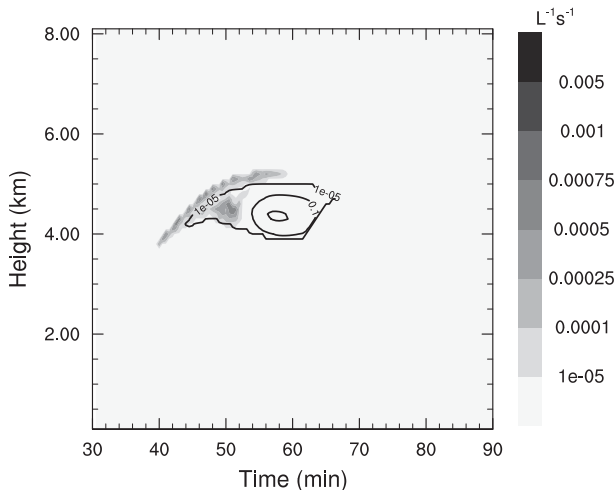
FIG. 5. Spatial and temporal evolution of the primary ice nucleation rate (L^{-1} s^{-1}, shaded area), and the ice splinter production rate (L^{-1} s^{-1}, solid lines) in the inner cylinder for the case E_4.

the ice particles containing ice-nucleating bacteria that may initiate ice formation or be scavenged by secondary ice particles. Concentrations of ice particles as large as 155 L^{-1} appeared in the dissipating stage (Fig. 6a), implying that a low concentration of IN can trigger ice multiplication. The primary nucleation of ascending small raindrops produces rimers (Fig. 6b) that result in ice crystal bursts via the H–M mechanism (Sun et al. 2010). The ice crystal multiplication process is directly influenced by the concentration of ice pellets. The initiation time and concentration of primary ice pellets are two determining factors that affect the production of ice bursts. These two factors are determined by both the production of primary ice particles and the evolution of raindrops. The concentration of primary ice pellets at the beginning of ice formation may be approximately estimated from the comparison between the total ice pellet concentration and the IN-containing ice pellet concentration. If the difference between them is small, then we can conclude that they represent the concentration of primary ice pellets that include ice pellets from small raindrop nucleation by ice-nucleating bacteria and from small raindrop nucleation by IN-containing ice particles. If the concentration of total ice pellets is highly greater than that of IN-containing ice pellets, then the production of the secondary ice pellets nucleated by the ejection of ice splinters becomes pronounced. Since bacteria-containing secondary ice pellets only occur when ice splinters collide with bacteria-containing raindrops or in a collision of secondary ice pellets with interstitial bacteria and bacteria-containing particles, bacteria-containing ice pellets may be regarded as bacteria-containing primary ice pellets or IN-containing ice pellets when the

total concentration of ice pellets is close to that of bacteria-containing ice pellets. Hence, we can use the concentration of bacteria-containing ice pellets instead of IN-containing ice pellets to determine the primary ice pellets in the ice initiation stage. Figure 6b shows the evolution of the concentration of the bacteria-containing ice pellets and the total concentration of ice pellets. In the dominant stage of the primary ice production, there is little difference between them and their concentrations are far less than the concentration of ice-nucleating bacteria. However, in the dominate stage of secondary ice production, the concentration of the total ice pellets is much greater than that of the bacteria-containing ice pellets. The ice pellet band is finally formed through the nucleation of the small raindrop band and then the secondary ice production rate reaches its maximum value. These results indicate that a high concentration of ice particles can occur in WPSCCs when primary ice pellets appear even though their concentrations may be far less than those of ice-nucleating bacteria.

b. The impact of ice nucleus concentration on ice crystal multiplication

The production of primary ice pellets is influenced by the concentration of IN active at temperatures above $-10°C$. There are large uncertainties in the measurement of IN in this temperature range (Mohler et al. 2007), and the concentration of IN may be lower than the value we used in the simulation described above. To show the impact of ice nucleus concentration on ice bursts, we simulated the ice formation process with different ice nucleus concentrations (Table 2). The highest bacterial concentration is 27 L^{-1}, among which the concentration of ice-nucleating bacteria is 0.27 L^{-1}; and the lowest bacterial concentration is 0.27 L^{-1}, among which the concentration of ice-nucleating bacteria is 0.0027 L^{-1} at $-10°C$. Table 3 shows the maximum ice particle concentrations, MPINR and MISPR values. The ice multiplication process occurred in all the simulations. The MPINR values increase with an increase of bacterial concentration. However, the MISPR values change slightly with an increase of bacterial concentration. These results indicate that ice multiplication in WPSCCs is insensitive to the concentration of IN. Figures 6c and 6d show the maximum concentration of ice particles and ice pellets in the simulation with a bacterial concentration of 0.27 L^{-1}. The maximum concentration of bacteria-containing ice particles is 0.02 L^{-1} (Fig. 6c), which includes both ice particles that contain and do not contain ice-nucleating bacteria. We also simulated this case with the riming process omitted. The results show that the concentration of ice particles and the concentration of bacteria-containing
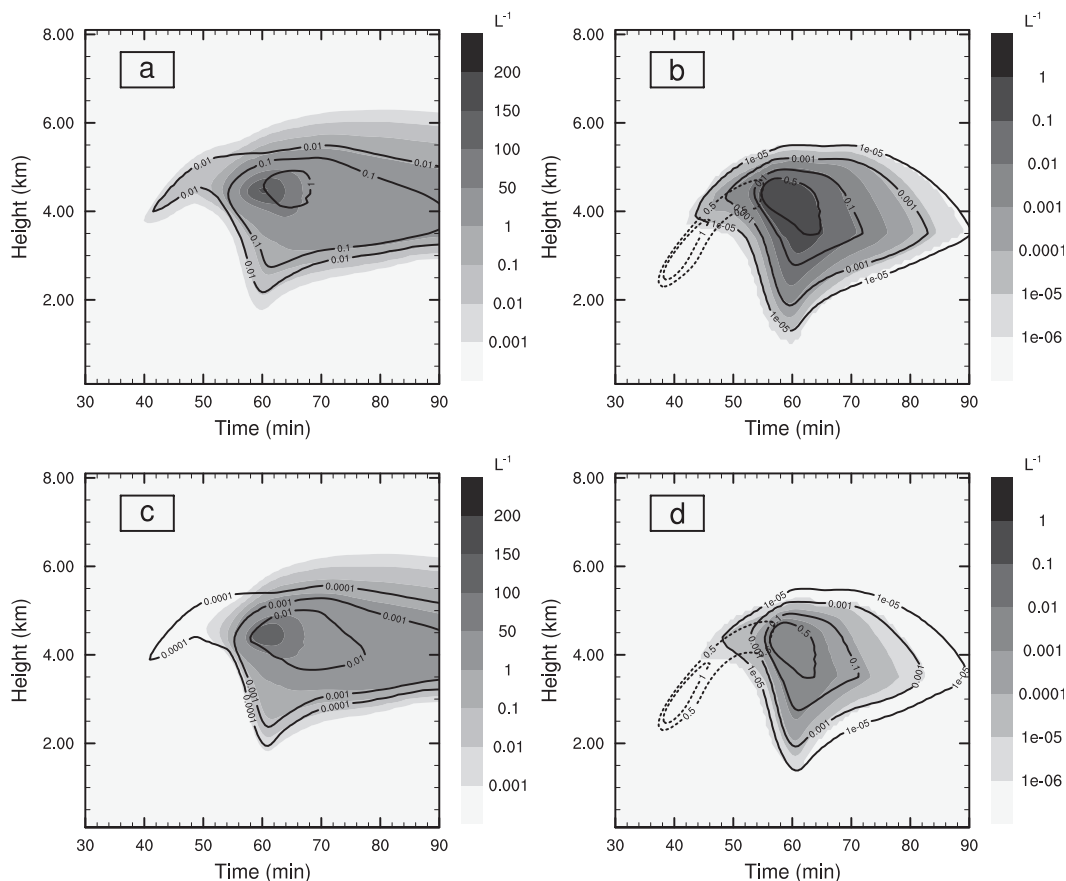
FIG. 6. Spatial and temporal evolution of small raindrops, ice particles, and ice pellets in the condensation and immersion freezing modes in the inner cylinder for cases (a),(b) E_4 and (c),(d) E_1. (a),(c) Ice particles (L^{-1}, shaded area) and bacteria-containing ice particles (L^{-1}, solid lines). (b),(d) Small raindrops (L^{-1}, dotted lines) and ice pellets (L^{-1}, solid lines), and bacteria-containing ice pellets (L^{-1}, shaded area).

ice particles are the same and only reach 3.0×10^{-4} L^{-1} because there is no secondary ice particle formation. These results indicate that out of the initial ice-nucleating bacteria concentration of 2.7×10^{-3} L^{-1}, a concentration of 3.0×10^{-4} L^{-1} was activated. The maximum concentration of activated ice-nucleating bacteria in experiment E_1 may be approximately one-tenth of their initial concentration or even less due to the scavenging of secondary ice particles. The small raindrop band is also nucleated even though the MPINR value is as low as 1.7×10^{-5} L^{-1} s^{-1} (Fig. 6d).

Table 3 in the experiments from E_1 to E_5 demonstrates that there is little difference in the maximum concentration of ice crystals for different bacterial concentrations if ice multiplication occurs. Our simulations also show that the impact of ice nucleus concentration on the ice concentration in WPSCCs is little if the small raindrop band reaches the ice multiplication temperature zone.

6. Sensitivity study of the effects of aerosol concentrations on ice formation in WPSCCs

The impacts of aerosols on the microphysics of deep convective clouds have been studied in recent years (Khain and Pokrovsky 2004; Khain et al. 2004, 2005; Cui et al. 2006; van den Heever et al. 2006; Lee et al. 2009).

TABLE 3. Simulation results.

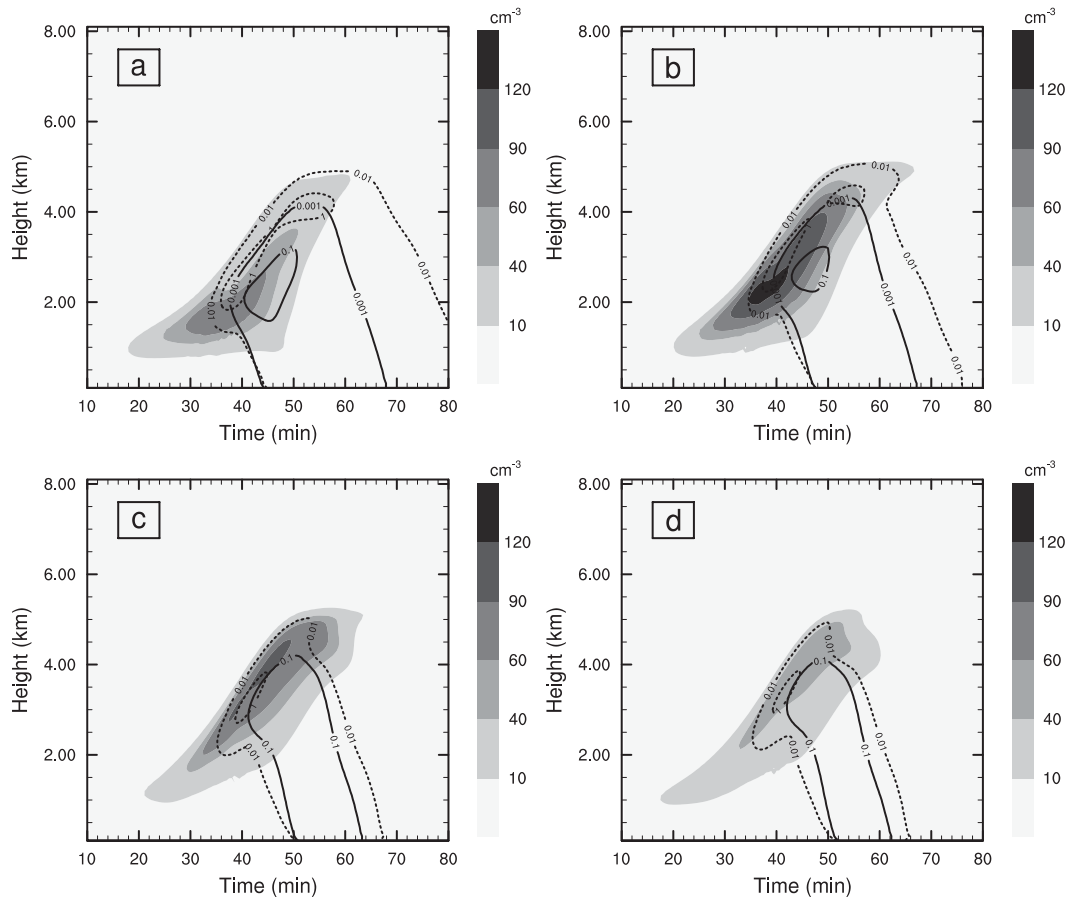| Case	Maximum ice concentration (L^{-1})	MPINR (L^{-1} s^{-1})	MISPR (L^{-1} s^{-1})
E_1	139.243	1.741×10^{-5}	1.239
E_2	146.904	8.661×10^{-5}	1.249
E_3	153.175	5.419×10^{-4}	1.219
E_4	155.337	1.038×10^{-3}	1.206
E_5	157.316	1.954×10^{-3}	1.198
E_6	0.098	8.901×10^{-4}	8.853×10^{-4}
E_7	30.011	9.347×10^{-4}	0.300
E_8	261.551	1.138×10^{-3}	1.654
E_9	549.649	1.063×10^{-3}	5.099

FIG. 7. Spatial and temporal evolution of water drop concentrations in the inner cylinder for the cases of (a) E_6, (b) E_7, (c) E_8, and (d) E_9 in different size categories. Cloud drops with diameters > 24.0 μm (cm^{-3}, shaded area), small raindrops with diameters > 600 μm (L^{-1}, dotted lines), and raindrops with diameters > 2 mm (m^{-3}, solid lines).

However, high concentrations of ice crystals have been observed in the dissipating stage of WPSCCs (Mossop 1985; Hobbs and Rangno 1985; Rangno and Hobbs 1991; Blyth and Latham 1993; Rangno and Hobbs 2005). The role of aerosols in these clouds will be quite different than that in deep convective clouds. For example, the H–M mechanism is not a dominant source of ice particles in deep clouds, but it may be a dominant process in WPSCCs.

Ice crystal bursts occur in both maritime and continental WPSCCs even though the aerosol concentrations in them are different (Hallett et al. 1978; Hobbs and Rangno 1985; Rangno and Hobbs 1991; Blyth and Latham 1993; Rangno and Hobbs 2005). High aerosol concentration has not been observed to delay ice formation in continental WPSCCs. Teller and Levin (2006) showed that polluted shallow cumulus clouds may have high concentrations of ice particles. These facts suggest the importance of improving our understanding of

the relationship between aerosol concentration and ice formation. The sensitivity simulations were run for five different scenarios of aerosol concentrations. These five cases are characterized as different air pollution situations.

a. Effect on cloud drop spectra and precipitation

The spatial and temporal evolution of cloud drop spectra depends on both cloud microphysics and dynamics and the interaction between them. For the same meteorological conditions, since water vapor supplies will be basically unchanged, an increase in cloud condensation nucleus concentration will result in a decrease in cloud drop sizes. Consequently, the height of the centers of maximum concentration of large cloud drops (diameters greater than 24 μm) increases with increasing aerosol concentration (Fig. 7). However, the concentration of large droplets increases with an increase of aerosol concentration and then decreases with
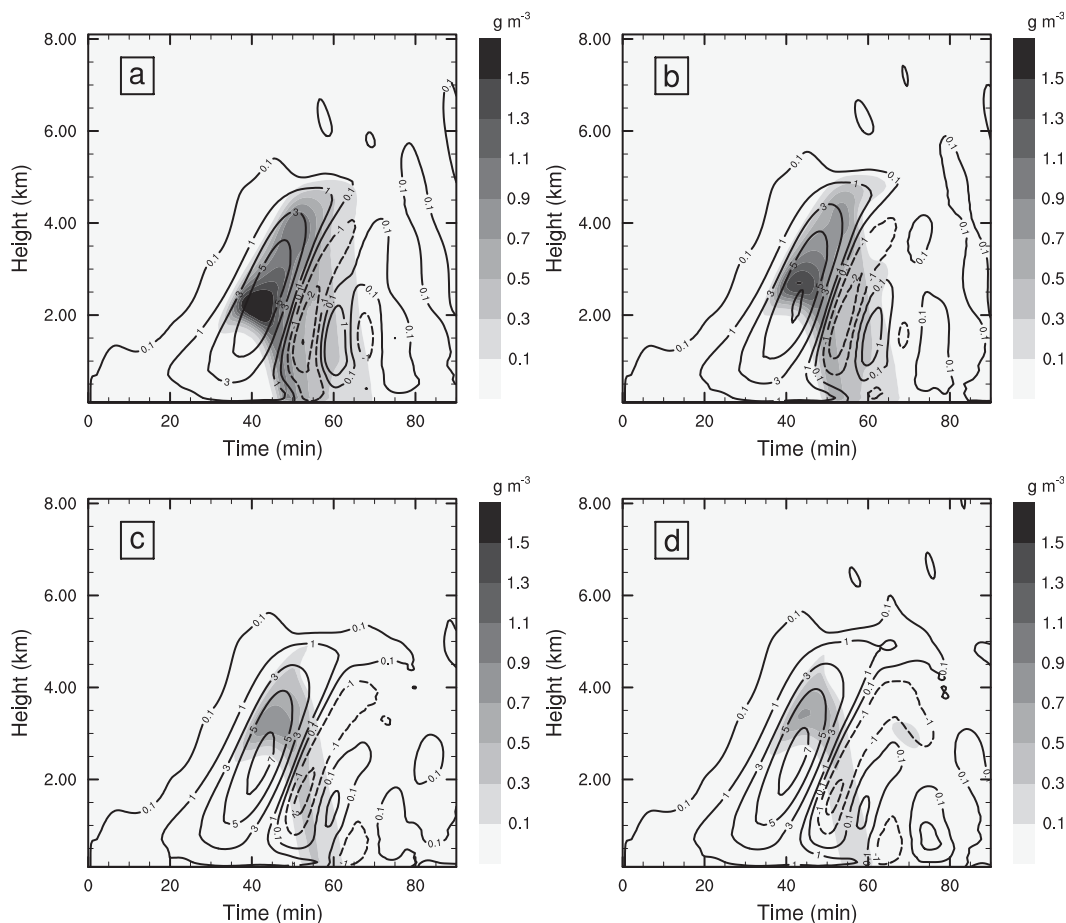
FIG. 8. Spatial and temporal evolution of vertical velocity (m s^{-1}, solid and dash lines) and rainwater content (diameter > 100 μm) (g m^{-3}, shaded area) in the inner cylinder for the cases of (a) E$_6$, (b) E$_7$, (c) E$_8$, and (d) E$_9$.

a further increase of aerosol concentration. Both the lowest concentration and highest concentration of aerosols result in low concentrations of large cloud drops. The decrease in size of cloud droplets leads to a delayed appearance of drizzle drops (diameters greater than 100 μm) and decreased concentrations of them (Fig. 7). As a result, both concentrations of raindrops and the rainwater content decrease with increasing concentrations of CCN beyond some optimum value, and precipitation is delayed (Figs. 3a, 4a, 7, and 8). An increase of aerosol concentration with multiples of the maritime aerosol concentration can suppress precipitation in WPSCCs (Figs. 3a and 8). This result is consistent with that of 3D simulations for such clouds (Feingold et al. 2005; Khain et al. 2008).

b. Effect on ice crystal spectra

With an increase in aerosol concentration, the concentration of ice pellets generated by the freezing of raindrops may decrease due to the decrease in the concentrations of raindrops (diameters greater than 600 μm) (Fig. 7). However, ice multiplication is also highly related to the concentration of cloud droplets available to be rimed by ice pellets. Table 3 in the experiments from E$_6$ to E$_9$ shows that the maximum concentration of ice particles increases with an increase in concentration of CCN with little changes in MPINR and big changes in MISPR. The total concentration of large ice particles (diameters greater than 150 μm) increases through the riming process when high concentrations of cloud drops are present in the clouds (Fig. 9). The concentrations of ice crystals are not proportional to those of ice pellets and increase with increasing concentrations of CCN. This is because ice splinter production rates increase with the increasing concentrations of cloud droplets if the cloud droplet spectra still meet the requirements of the mechanism, even though the ice pellet concentrations decrease. Figure 8 also shows the concentration of ice crystals with diameters less than 20 μm, which includes primary ice crystals from condensation

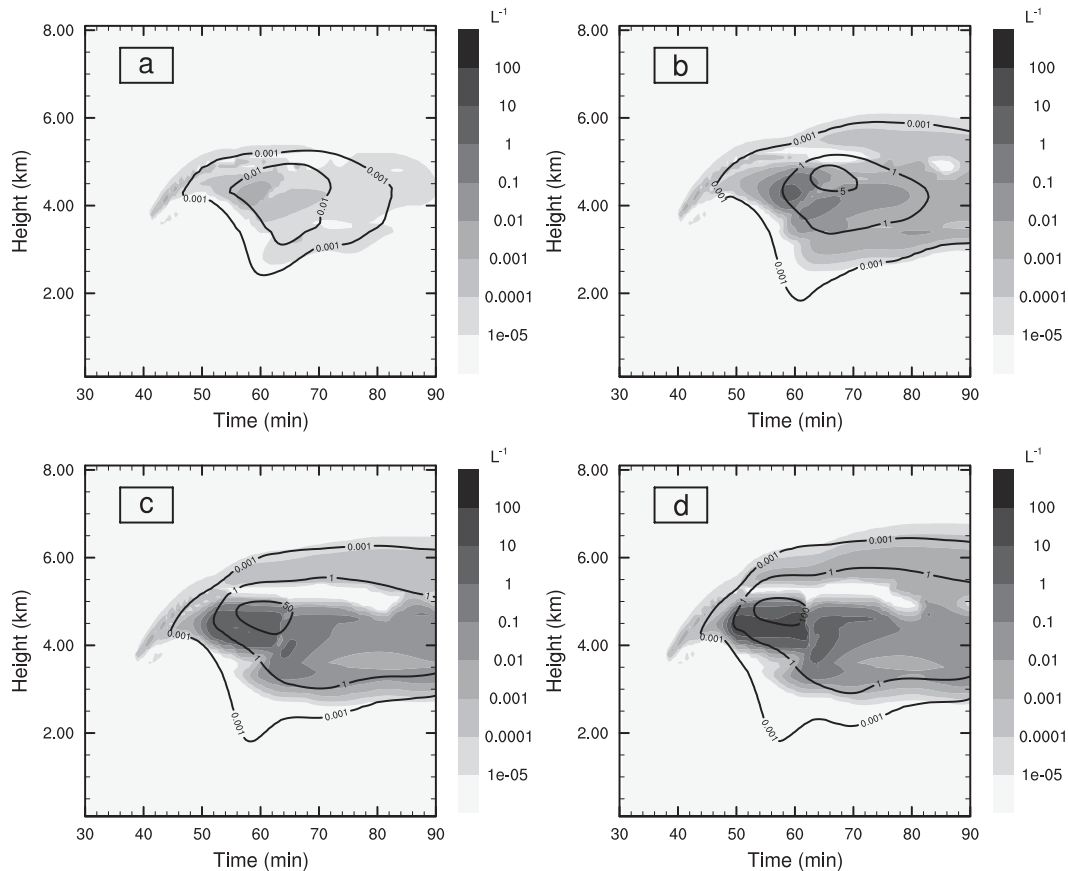FIG. 9. Spatial and temporal evolution of ice particle concentrations in the inner cylinder for the cases of (a) E_6, (b) E_7, (c) E_8, and (d) E_9 in different size categories. Small ice concentration (diameter < 20 μm) (L^{-1}, shaded area) and large ice concentration (diameter > 150 μm) (L^{-1}, solid lines).

freezing at the cloud top, ice splinters produced in the zone, and small melted ice particles near the cloud base. The maximum values of ice splinter concentrations increase from 1.0×10^{-4} to 1.0 L^{-1}. Since high aerosol concentrations result in high concentrations of cloud drops, the ice splinter production rates for the cases with higher aerosol concentrations are larger than those for the cases with smaller ones if the cloud drop-size distribution meets the requirements for the mechanism to be effective. However, it should be noted that there must be an aerosol concentration limit beyond which riming efficiencies are reduced, so that the mechanism becomes ineffective.

c. Effect on the ice water content and dynamics

With the concentration of the riming-dominant ice particles increasing (Fig. 9), the ice water contents increase with an increase of the aerosol concentration. The maximum ice water content increases from 0.07 to more than 1.7 g m^{-3} in continental polluted conditions. The resulting increase in latent heat release leads to strengthened

updrafts in the upper part of clouds (Fig. 8). In addition, there are small increases in updraft at lower levels in the cloud due to reduced precipitation drag in the simulations with higher aerosol concentrations. However, with a low concentration of aerosols, more precipitation drag leads to a strong downdraft, which in turn triggers a relatively strong secondary convection (Fig. 8). The interaction between aerosols and cumulus clouds is a process involving both microphysics and dynamics. The impact of aerosols on the microphysics and precipitation has been understood in combination with the dynamical fields of cumulus clouds (Khain et al. 2005; Tao et al. 2007; Khain et al. 2008). It should be noted that ambient wind shear has not been considered in our 1.5D model. It should also be noted that the temperature of cloud base is more than 15°C in our case study. If the height of cloud base increases, then the concentration of raindrops is expected to decrease, the precipitation efficiency of such WPSCCs will be lower than those of the thicker WPSCCs we simulated, and the ice concentration will also decrease.
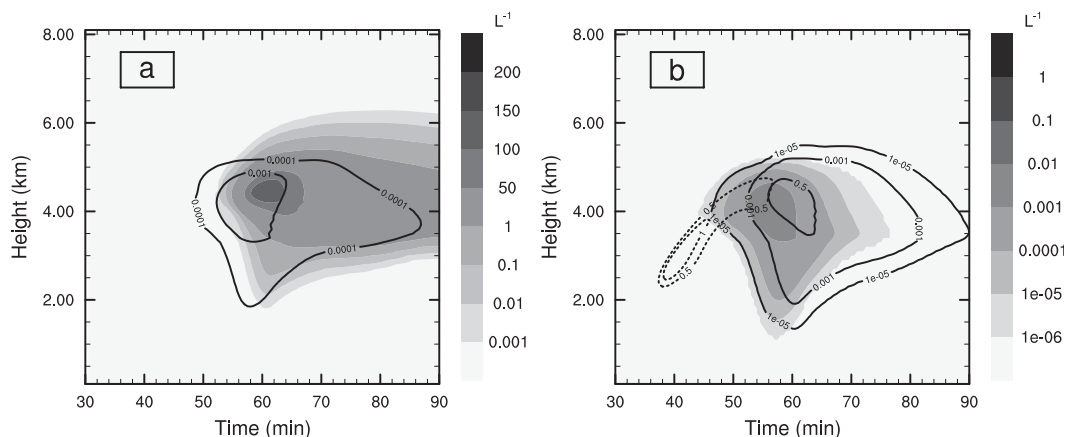
FIG. 10. Spatial and temporal evolution of small raindrops, ice particles, and ice pellets in the inner cylinder in the immersion freezing mode with ice-nucleating bacterial concentration of 0.135 L^{-1}. (a) Ice particles (L^{-1}, shaded area) and bacteria-containing ice particles (L^{-1}, solid lines). (b) Small raindrops (L^{-1}, dotted lines) and ice pellets (L^{-1}, solid lines), and bacteria-containing ice pellets (L^{-1}, shaded area).

7. Simulations based on a laboratory constraint parameterization

Diehl and Wurzler (2004) proposed a parameterization constrained by results from laboratory experiments for different IN acting via the immersion freezing mode. The freezing of a water drop containing a specific ice nucleus is independent of the size of the IN and is based on a median freezing temperature that was derived from laboratory experiments. The Diehl and Wurzler parameterization is a function of temperature, ice nucleus composition, droplet volume, the cooling rate of clouds, and the concentration of soluble material in cloud droplets. It should be noted that insoluble aerosols implemented into the model only refer to ice-nucleating aerosols and exclude non-ice-nucleating aerosols in this parameterization scheme. We repeated the experiment of E_4 with a concentration of ice-nucleating bacteria of 0.135 L^{-1} and the IN only acting through the immersion freezing mode.

Different nucleation modes can lead to different concentrations of primary ice particles in different regions of cumulus clouds. Figure 10 shows ice particle concentrations from this simulation. The maximum concentration of total ice particles and bacteria-containing ice particles reaches 140 and 0.002 L^{-1} (Fig. 10a), respectively. Note that ice formation at the cloud top is delayed due to the absence of condensation nucleation. The maximum concentrations of both ice particles and bacteria-containing ice particles are less than those from the simulation that includes both condensation nucleation and immersion nucleation in the experiment E_4 with the observational-constraint parameterization approach. This result is consistent with the simulation with a parcel

model [see Eidhammer et al. (2009), their Fig. 7]. The parameterization of Diehl and Wurzler (2004) might underestimate ice concentrations at relatively warm temperatures. This result further indicates that condensation freezing at cloud top is also an important pathway for ice formation in cumulus clouds.

The above-mentioned modeling results imply that ice-nucleating bioaerosols can trigger the ice multiplication process in WPSCCs under different assumed ice nucleation parameterizations. However, ice multiplication in WPSCCs is also determined by many other factors (Sun et al. 2010), among which a small raindrop band plays a very important role. The concentration of small raindrops and the location of the small raindrop band are determined by both dynamical and microphysical processes. The initial temperature and humidity profiles and the environmental wind field all impact raindrop formation. Therefore, further in situ observations are needed in future.

8. Conclusions

We simulated ice initiation and ice multiplication in WPSCCs. Our results indicate that ice multiplication in these kinds of clouds can be explained by the H–M mechanism. The impacts of various microphysical processes on this mechanism have been evaluated. Different ice initiation mechanisms, ice nucleus concentrations, and concentrations of CCN all affect the ice multiplication process. However, a supercooled small raindrop band plays a central role in ice multiplication (Sun et al. 2010). The formation of raindrops and their subsequent freezing is a precondition for ice crystal bursts in WPSCCs. The idea of nucleation of supercooled raindrops to accelerate ice multiplication was proposed by Hallett et al. (1978)

several decades ago. Sun (2008) further proposed that there should be an upward-moving small raindrop band within cumulus clouds. Other factors affect the timing and the magnitude of ice multiplication.

The involvement of the ice multiplication mechanism leads to an additional way of ice formation in WPSCCs. An increase in the concentration of CCN in these kinds of clouds does not necessarily delay ice formation, even though the sizes of cloud drops become smaller. Moreover, the undelayed onset of ice crystal formation results in the formation of a greater ice water content through the riming process because more cloud drops are available at subfreezing heights. As a result, the development of clouds will be strengthened because of more latent heat release compared to clouds forming in environments with smaller concentrations of CCN. Therefore, the thermodynamic effect (Hegerl et al. 2007; Romps and Kuang 2010) that impacts the development of deep cumulus clouds is still meaningful for WPSCCs, but the mechanisms are different. Furthermore, an increase in the concentration of CCN can weaken the secondary convection, since the compensating downdraft of the initial convection will become less strong due to a reduced warm-rain precipitation drag.

Ice concentrations in WPSCCs are related to the concentrations of both CCN and IN. Ice-nucleating bacteria can trigger ice multiplication even though their concentrations are very small. Other ice-nucleating bioaerosols, such as fungi, pollen, and leaf debris, may also trigger ice multiplication (Sun 2008) even though there are no reports of in situ observations of their concentrations. Ice-nucleating bioaerosols dominate ice initiation at temperatures warmer than $-8°C$. Therefore, any parameterization of ice formation should consider bioaerosols' effects on ice formation.

Our findings concerning the evolution of cumulus cloud spectra and the ice initiation and multiplication processes are based on a 1.5D nonhydrostatic convective cloud and aerosol interaction model. It should be emphasized that the 1D framework imposes some constraints on the generality of our results. A 1D framework cannot consider the impacts of environmental wind shear on the evolution of cloud drop spectra. Environmental wind shear can strengthen the lateral entrainment. Depending on whether the entrained air is dry or wet may affect the microphysics in different ways. Furthermore, there is evidence that a thin subsiding shell surrounds the cumulus cloud boundary (Rodts et al. 2003). Our model has only a simplified vortex circulation at cloud top and lateral mixing, which impacts the cloud physics. These deficiencies should be addressed in future studies, including numerical experiments in the framework of a 3D cloud model with bin-resolved microphysics.

APPENDIX A

Explicit Expression for Microphysical Processes of CCN

With specific expressions for the microphysical processes of CCN, the number density distributions of hydrometeors with water mass m and CCN mass m_{ap}, $f_{wat}(m, m_{ap})$ and $f_{ice}(m, m_{ap})$ are calculated by numerical integration of the following two equations:

$$
\begin{aligned}
\left.\frac{\partial f_{wat}(m, m_{ap})}{\partial t}\right|_{mic} = & -\frac{\partial\left[f_{wat}(m, m_{ap})\left.\frac{dm}{dt}\right|_{wat}\right]}{\partial m} - f_{wat}(m, m_{ap})R_{hetero}(m) \\
& - \int_{m_{0ice}}^{\infty} f_{wat}(m, m_{ap}) \int_{m_{ap0}}^{\infty} K(m', m)f_{ice}(m', m'_{ap}) \, dm'_{ap} \, dm' \\
& - \int_{m_{0drop}}^{\infty} f_{wat}(m, m_{ap}) \int_{m_{ap0}}^{\infty} K(m, m')f_{wat}(m', m'_{ap}) \, dm'_{ap} \, dm' \\
& + \int_{m_{0drop}}^{m/2} \int_{m_{ap0}}^{m_{ap}/2} f_{wat}(m - m', m_{ap} - m'_{ap})K(m - m', m')f_{wat}(m', m'_{ap}) \, dm'_{ap} \, dm' \\
& + \frac{\partial\left[f_{ice}(m, m_{ap})\left.\frac{dm}{dt}\right|_{melting}\right]}{\partial m}
\end{aligned}
$$

(A1)

$$\left.\frac{\partial f_{ice}(m, m_{ap})}{\partial t}\right|_{mic} = -\frac{\partial\left[f_{ice}(m, m_{ap})\left.\frac{dm}{dt}\right|_{ice}\right]}{\partial m} + f_{wat}(m, m_{ap})R_{hetero}(m)$$

$$- \int_{m_{0drop}}^{\infty} f_{ice}(m, m_{ap}) \int_{m_{ap0}}^{\infty} K(m, m_{drop})f_{wat}(m_{drop}, m'_{ap}) \, dm'_{ap} \, dm_{drop}$$

$$+ \int_{m_{0drop}}^{m - m_{0ice}} \int_{m_{ap0}}^{m_{ap} - m_{ap0}} f_{wat}(m_{drop}, m'_{ap})K(m - m_{drop}, m_{drop})f_{ice}(m - m_{drop}, m_{ap} - m'_{ap}) \, dm'_{ap} \, dm_{drop}$$

$$- \int_{m_{0ice}}^{\infty} f_{ice}(m, m_{ap}) \int_{m_{ap0}}^{\infty} K(m, m')Esf_{ice}(m', m'_{ap}) \, dm'_{ap} \, dm'$$

$$+ \int_{m_{0ice}}^{m/2} \int_{m_{ap0}}^{m_{ap}/2} f_{ice}(m - m', m_{ap} - m'_{ap})K(m - m', m')Esf_{ice}(m', m'_{ap}) \, dm'_{ap} \, dm'$$

$$- \frac{\partial\left[f_{ice}(m, m_{ap})\left.\frac{dm}{dt}\right|_{melting}\right]}{\partial m}, \tag{A2}$$

where m_{0ice} is the minimum mass of ice crystals, m_{0drop} is the minimum mass of water drops, and m_{ap0} is the minimum mass of CCN in all ice and water particles; $R(m)$ is the drop freezing rate for a drop with water mass m; k is the collection kernel between the two particles (Sun 2008). Es is the sticking efficiency between the two ice particles; we assumed that Es is 0.3 given by Latham and Saunders (1970). The flux method for finding the numerical solution of the stochastic collection process of the masses of both aerosol and water is presented by Bott (2000). This method is based on the assumption that the probability for the collision of two hydrometeors (ice or water) only depends on the water mass of them. However, in our simulations, the collection kernel between two hydrometeors depends on both their water mass and aerosol mass, which may slightly impact the aerosol redistribution after a collision. We assumed that the ice nucleation capabilities for drops with identical water mass but with different masses of CCN are the same. Under such an assumption, we can derive the freezing rates of drops containing CCN through that of drops containing IN as follows:

$$R_{hetero}(m) = \frac{\int_{0}^{\infty} R_{hetero}(m, m_{IN})g_{wat}(m, m_{IN}) \, dm_{IN}}{\int_{0}^{\infty} f(m, m_{ap}) \, dm_{ap}}. \tag{A3}$$

APPENDIX B

Explicit Expression for Microphysical Processes of IN

To determine changes in $g_{wat}(m, m_{IN})$ and $g_{ice}(m, m_{IN})$ due to riming and coalescence in which IN and IN-containing hydrometeors may collide with IN-free hydrometeors, we assumed that m_{IN} in $g_{wat}(m, m_{IN})/g_{ice}(m, m_{IN})$ is equal to zero if water droplets/ice particles contain no IN as shown:

$$g_{wat}(m, m_{IN} = 0) = \int_{m_{ap0}}^{\infty} f_{wat}(m, m'_{ap}) \, dm'_{ap}$$
$$- \int_{m_{IN0}}^{\infty} g_{wat}(m, m'_{IN}) \, dm'_{IN} \tag{B1}$$

$$g_{ice}(m, m_{IN} = 0) = \int_{m_{ap0}}^{\infty} f_{ice}(m, m'_{ap}) \, dm'_{ap}$$
$$- \int_{m_{IN0}}^{\infty} g_{ice}(m, m'_{IN}) \, dm'_{IN}, \tag{B2}$$

where m_{IN0} is the mass of the smallest ice nucleus.

For the hydrometeors containing IN with mass $m_{IN} \neq 0$, $g_{wat}(m, m_{IN})$ and $g_{ice}(m, m_{IN})$ are calculated by numerical integration of the following equations:

$$
\begin{aligned}
\left.\frac{\partial g_{\text{wat}}(m,m_{\text{IN}})}{\partial t}\right|_{\text{mic}} = & -\frac{\partial\left[g_{\text{wat}}(m,m_{\text{IN}})\left.\dfrac{dm}{dt}\right|_{\text{wat}}\right]}{\partial m} - g_{\text{wat}}(m,m_{\text{IN}})R_{\text{hetero}}(m,m_{\text{IN}}) \\
& - \int_{m_{0\text{ice}}}^{\infty} g_{\text{wat}}(m,m_{\text{IN}})\int_{0}^{\infty} K(m_{\text{ice}},m)g_{\text{ice}}(m_{\text{ice}},m'_{\text{IN}})\,dm'_{\text{IN}}\,dm_{\text{ice}} \\
& - \int_{m_{0\text{drop}}}^{\infty} g_{\text{wat}}(m,m_{\text{IN}})\int_{0}^{\infty} K(m,m_{\text{drop}})g_{\text{wat}}(m_{\text{drop}},m'_{\text{IN}})\,dm'_{\text{IN}}\,dm_{\text{drop}} \\
& + \int_{m_{0\text{drop}}}^{m/2}\int_{0}^{m_{IN}/2} g_{\text{wat}}(m_{\text{drop}},m'_{\text{IN}})K(m-m_{\text{drop}},m_{\text{drop}})g_{\text{wat}}(m-m_{\text{drop}},m_{\text{IN}}-m'_{\text{IN}})\,dm'_{\text{IN}}\,dm_{\text{drop}} \\
& + \frac{\partial\left[g_{\text{ice}}(m,m_{\text{IN}})\left.\dfrac{dm}{dt}\right|_{\text{melting}}\right]}{\partial m}
\end{aligned}
\tag{B3}
$$

$$
\begin{aligned}
\left.\frac{\partial g_{\text{ice}}(m,m_{\text{IN}})}{\partial t}\right|_{\text{mic}} = & -\frac{\partial\left[g_{\text{ice}}(m,m_{\text{IN}})\left.\dfrac{dm}{dt}\right|_{\text{ice}}\right]}{\partial m} + g_{\text{wat}}(m)R_{\text{hetero}}(m,m_{\text{IN}}) \\
& - \int_{m_{0\text{drop}}}^{\infty} g_{\text{ice}}(m,m_{\text{IN}})\int_{0}^{\infty} K(m,m_{\text{drop}})g_{\text{wat}}(m_{\text{drop}},m'_{\text{IN}})\,dm'_{\text{IN}}\,dm_{\text{drop}} \\
& + \int_{m_{0\text{drop}}}^{m-m_{0\text{crys}}}\int_{0}^{m_{\text{IN}}} g_{\text{wat}}(m_{\text{drop}},m'_{\text{IN}})K(m-m_{\text{drop}},m_{\text{drop}})g_{\text{ice}}(m-m_{\text{drop}},m_{\text{IN}}-m'_{\text{IN}})\,dm'_{\text{IN}}\,dm_{\text{drop}} \\
& - \int_{m_{0\text{ice}}}^{\infty} g_{\text{ice}}(m,m_{\text{IN}})\int_{0}^{\infty} K(m,m_{\text{ice}})\text{E}sg_{\text{ice}}(m_{\text{ice}},m'_{\text{IN}})\,dm'_{\text{IN}}\,dm_{\text{ice}} \\
& + \int_{m_{0}}^{m/2}\int_{0}^{m_{\text{IN}}/2} g_{\text{ice}}(m_{\text{ice}},m'_{\text{IN}})K(m-m_{\text{ice}},m_{\text{ice}})\text{E}sg_{\text{ice}}(m-m_{\text{ice}},m_{\text{IN}}-m'_{\text{IN}})\,dm'_{\text{IN}}\,dm_{\text{ice}} \\
& - \frac{\partial\left[g_{\text{ice}}(m,m_{\text{IN}})\left.\dfrac{dm}{dt}\right|_{\text{melting}}\right]}{\partial m}.
\end{aligned}
\tag{B4}
$$

APPENDIX C

Parameterization Scheme for the Secondary Ice Production Rate

The secondary ice production rate parameterized by Harris-Hobbs and Cooper (1987) is determined as follows:

$$
\begin{aligned}
P = Cf(T)\int_{r_0}^{\infty}\int_{R_0}^{\infty} & g(R)\pi(R+r)^2[V(R) \\
& -v(r)]N(R)n(r)E(R,r)\,dR\,dr
\end{aligned}
\tag{C1}
$$

$$
f(T) = -(T+3)/2, \quad -3° > T \geq -5°\text{C} \tag{C2}
$$

$$
f(T) = (T+8)/3, \quad -5° \geq T > -8°\text{C} \tag{C3}
$$

$$
f(T) = 0, \quad \text{otherwise}, \tag{C4}
$$

where $E(R,r)$ is the collision efficiency between large ice particles and cloud drops; R, $V(R)$, and $N(R)$ are respectively the equivalent radius, terminal velocity, and size spectrum for large ice particles r, $v(r)$, and $n(r)$ are respectively the cloud droplet radius, terminal velocity, and size spectrum; and $g(R)$ represents the importance of small cloud particles ($5 <$ diameter $< 13~\mu$m) in the ice multiplication process, shown as

$$
g(R) = G_{<13}/G_{\text{all}} \tag{C5}
$$

$$
G_x = \int n(r)r^2E(R,r)\,dr, \tag{C6}
$$

where the limits of integration cover radii from 2.5 to 6.5 μm for $G_x = G_{13}$ and cover all droplet sizes for $G_x = G_{\text{all}}$, C is a constant, and $C = 0.21$.

The above-mentioned production rate of secondary ice particles P is determined according to the assumption that ice fragments are produced when large droplets (>24.0 μm in diameter) strike a portion of the rimed ice pellet's surface where small droplets (<13.0 μm) have accreted (Mossop and Wishart 1978). We applied this method in our modeling study.

REFERENCES

Ansmann, A., and Coauthors, 2008: Influence of Saharan dust on cloud glaciation in southern Morocco during the Saharan Mineral Dust Experiment. *J. Geophys. Res.,* **113,** D04210, doi:10.1029/2007JD008785.

Ariya, P. A., J. Sun, N. A. Eltouny, E. D. Hudson, C. T. Hayes, and G. Kos, 2009: Physical and chemical characterization of bioaerosols - Implications for nucleation processes. *Int. Rev. Phys. Chem.,* **28,** 1–32.

Asai, T., and A. Kasahara, 1967: A theoretical study of the compensating downward motions associated with cumulus clouds. *J. Atmos. Sci.,* **24,** 487–496.

Baker, M., 2001: Cloud physics: Inside history on droplets. *Nature,* **413,** 586–587.

Berezinski, N. A., G. V. Stepanov, and V. G. Khorguani, 1988: Ice-forming activity of atmospheric aerosol particles of different sizes. *Atmospheric Aerosols and Nucleation,* P. E. Wagner and G. Vali, Eds., Springer, 709–712.

Blyth, A. M., and J. Latham, 1993: Development of ice and precipitation in New Mexican summertime cumulus clouds. *Quart. J. Roy. Meteor. Soc.,* **119,** 91–120.

Bott, A., 2000: A flux method for the numerical solution of the stochastic collection equation: Extension to two-dimensional particle distributions. *J. Atmos. Sci.,* **57,** 284–294.

Bowers, R. M., C. L. Lauber, C. Wiedinmyer, M. Hamady, A. G. Hallerar, R. Fall, R. Knight, and N. Fierer, 2009: Characterization of airborne microbial communities at a high-elevation site and their potential to act as atmospheric ice nuclei. *Appl. Environ. Microbiol.,* **75,** 5121–5130.

——, S. McLetchie, R. Knight, and N. Fierer, 2010: Spatial variability in airborne bacterial communities across land-use types and their relationship to the bacterial communities of potential source environments. *ISME J.,* **5,** 601–612.

Burrows, S. M., W. Elbert, M. G. Lawrence, and U. Pöschl, 2009: Bacteria in the global atmosphere - Part 1: Review and synthesis of literature data for different ecosystems. *Atmos. Chem. Phys.,* **9,** 9263–9280.

Cardwell, J., P. R. Field, and T. W. Choularton, 2003: A modelling study of ice-spectrum modes in deep frontal clouds. *Quart. J. Roy. Meteor. Soc.,* **129,** 1873–1890.

Chen, Y., S. M. Kreidenweis, L. M. McInnes, D. C. Rogers, and P. J. DeMott, 1998: Single particle analyses of ice nucleating particles in the upper troposphere and lower stratosphere. *Geophys. Res. Lett.,* **25,** 1391–1394.

Chou, C., O. Stetzer, E. Weingartner, Z. Jurányi, Z. A. Kanji, and U. Lohmann, 2011: Ice nuclei properties within a Saharan dust event at the Jungfraujoch in the Swiss Alps. *Atmos. Chem. Phys.,* **11,** 4725–4738.

Choularton, T. W., J. Latham, and B. J. Mason, 1978: A possible mechanism of ice splinter production during riming. *Nature,* **274,** 791–792.

Christner, B. C., C. E. Morris, C. M. Foreman, R. Cai, and D. C. Sands, 2008: Ubiquity of biological ice nucleators in snowfall. *Science,* **319,** 1214, doi:10.1126/science.1149757.

Clarke, A. D., and Coauthors, 2004: Size distributions and mixtures of dust and black carbon aerosol in Asian outflow: Physiochemistry and optical properties. *J. Geophys. Res.,* **109,** D15S09, doi:10.1029/2003JD004378.

Connolly, P. J., O. Mohler, P. R. Field, H. Saathoff, R. Burgess, T. Choularton, and M. Gallagher, 2009: Studies of heterogeneous freezing by three different desert dust samples. *Atmos. Chem. Phys.,* **9,** 2805–2824.

Cui, Z., K. S. Carslaw, Y. Yin, and S. Davies, 2006: A numerical study of aerosol effects on the dynamics and microphysics of a deep convective cloud in a continental environment. *J. Geophys. Res.,* **111,** D05201, doi:10.1029/2005JD005981.

DeMott, P. J., and A. J. Prenni, 2010: New directions: Need for defining the numbers and sources of biological aerosols acting as ice nuclei. *Atmos. Environ.,* **44,** 1944–1945.

——, K. Sassen, M. R. Poellot, D. Baumgardner, D. C. Rogers, S. D. Brooks, A. J. Prenni, and S. M. Kreidenweis, 2003: African dust aerosols as atmospheric ice nuclei. *Geophys. Res. Lett.,* **30,** 1732, doi:10.1029/2003GL017410.

Després, V. R., and Coauthors, 2012: Primary biological aerosol particles in the atmosphere: A review. *Tellus,* **64B,** 15598, doi:10.3402/tellusb.v64i0.15598.

Diehl, K., and S. Wurzler, 2004: Heterogeneous drop freezing in the immersion model: Model calculations considering soluble and insoluble particles in the drops. *J. Atmos. Sci.,* **61,** 2063–2072.

——, and ——, 2010: Air parcel model simulations of a convective cloud: Bacteria acting as immersion ice nuclei. *Atmos. Environ.,* **44,** 4622–4628.

Dye, J. E., and Coauthors, 1986: Early electrification and precipitation development in a small, isolated Montana cumulonimbus. *J. Geophys. Res.,* **91,** 1231–1247.

Dymarska, M., B. J. Murray, L. Sun, M. L. Eastwood, D. A. Knopf, and A. K. Bertram, 2006: Deposition ice nucleation on soot at temperatures relevant for the lower troposphere. *J. Geophys. Res.,* **111,** D04204, doi:10.1029/2005JD006627.

Eidhammer, T., P. J. DeMott, and S. M. Kreidenweis, 2009: A comparison of heterogeneous ice nucleation parameterizations using a parcel model framework. *J. Geophys. Res.,* **114,** D06202, doi:10.1029/2008JD011095.

Feingold, G., H. Jiang, and J. Y. Harrington, 2005: On smoke suppression of clouds in Amazonia. *Geophys. Res. Lett.,* **32,** L02804, doi:10.1029/2004GL021369.

Franc, G. D., and P. J. DeMott, 1998: Cloud activation characteristics of airborne *Erwinia carotovora* cells. *J. Appl. Meteor.,* **37,** 1293–1300.

Gross, D. C., Y. S. Cody, E. L. Proebsting, G. K. Radamaker, and R. A. Spotts, 1983: Distribution, population dynamics, and characteristics of ice nucleation-active bacteria in deciduous fruit tree orchards. *Appl. Environ. Microbiol.,* **46,** 1370–1379.

Hallett, J., R. I. Sax, D. Lamb, and A. S. R. Murty, 1978: Aircraft measurements of ice in Florida cumuli. *Quart. J. Roy. Meteor. Soc.,* **104,** 631–651.

Harris-Hobbs, R. L., and W. A. Cooper, 1987: Field evidence supporting quantitative predictions of secondary ice production rates. *J. Atmos. Sci.,* **44,** 1071–1082.

Hegerl, G. C., and Coauthors, 2007: Understanding and attributing climate change. *Climate Change 2007: The Physical Science Basis,* S. Solomon et al., Eds., Cambridge University Press, 663–745.

Heymsfield, A. J., and S. C. Mossop, 1984: Temperature dependence of secondary ice crystal production during soft hail growth by riming. *Quart. J. Roy. Meteor. Soc.,* **110,** 765–770.

——, and L. M. Miloshevich, 1993: Homogeneous ice nucleation and supercooled liquid water in orographic wave clouds. *J. Atmos. Sci.,* **50,** 2335–2353.

Hobbs, P. V., and A. L. Rangno, 1985: Ice particle concentrations in clouds. *J. Atmos. Sci.,* **42,** 2523–2449.

——, and ——, 1990: Rapid development of ice particle concentrations in small, polar maritime cumuliform clouds. *J. Atmos. Sci.,* **47,** 2710–2722.

——, and ——, 1998: Reply to "Comments by Alan M. Blyth and John Latham on 'Cumulus glaciation papers by P. V. Hobbs and A. L. Rangno.'" *Quart. J. Roy. Meteor. Soc.,* **124,** 1009–1011.

Holton, J. R., 1973: A one-dimensional cumulus model including pressure perturbations. *Mon. Wea. Rev.,* **101,** 201–205.

Hoose, C., J. E. Kristjansson, and S. M. Burrows, 2010a: How important is biological ice nucleation in clouds on a global scale? *Environ. Res. Lett.,* **5,** 024009, doi:10.1088/1748-9326/5/2/024009.

——, ——, J.-P. Chen, and A. Hazra, 2010b: A classical-theory-based parameterization of heterogeneous ice nucleation by mineral dust, soot, and biological particles in a global climate model. *J. Atmos. Sci.,* **67,** 2483–2503.

Jayaratne, E. R., and T. S. Verma, 2001: The impact of biomass burning on the environmental aerosol concentration in Gaborone, Botswana. *Atmos. Environ.,* **35,** 1821–1828.

Khain, A., and A. Pokrovsky, 2004: Simulation of effects of atmospheric aerosols on deep turbulent convective clouds using a spectral microphysics mixed-phase cumulus cloud model. Part II: Sensitivity study. *J. Atmos. Sci.,* **61,** 2983–3001.

——, ——, M. Pinsky, A. Seifert, and V. T. J. Phillips, 2004: Simulation of effects of atmospheric aerosols on deep turbulent convective clouds using a spectral microphysics mixed-phase cumulus cloud model. Part I: Model description and possible applications. *J. Atmos. Sci.,* **61,** 2963–2982.

——, D. Rosenfeld, and A. Pokrovsky, 2005: Aerosol impact on the dynamics and microphysics of deep convective clouds. *Quart. J. Roy. Meteor. Soc.,* **131,** 2639–2663.

——, N. BenMoshe, and A. Pokrovsky, 2008: Factors determining the impact of aerosols on surface precipitation from clouds: An attempt at classification. *J. Atmos. Sci.,* **65,** 1711–1748.

Klein, H., and Coauthors, 2010: Saharan dust and ice nuclei over central Europe. *Atmos. Chem. Phys.,* **10,** 10 211–10 221.

Knopf, D. A., P. A. Alpert, B. Wang, and J. Y. Aller, 2011: Stimulation of ice nucleation by marine diatoms. *Nat. Geosci.,* **4,** 88–90.

Koenig, L. R., 1963: The glaciating behavior of small cumulonimbus clouds. *J. Atmos. Sci.,* **20,** 27–47.

Latham, J., and W. P. R. Saunders, 1970: Experimental measurements of the collection efficiencies of ice crystals in electric fields. *Quart. J. Roy. Meteor. Soc.,* **96,** 255–265.

Lee, S. S., L. J. Donner, and V. T. J. Phillips, 2009: Impacts of aerosol chemical composition on microphysics and precipitation in deep convection. *Atmos. Res.,* **94,** 220–237.

Leroy, D., M. Monier, W. Wobrock, and A. I. Flossmann, 2006: A numerical study of the effects of the aerosol particle spectrum on the development of the ice phase and precipitation formation. *Atmos. Res.,* **80,** 15–45.

Lindemann, J., H. A. Constantinidou, W. R. Barchet, and C. D. Upper, 1982: Plants as sources of airborne bacteria including, ice nucleation-active bacteria. *Appl. Environ. Microbiol.,* **44,** 1059–1063.

List, R., and E. P. Lozowski, 1970: Pressure perturbation and buoyancy in convective clouds. *J. Atmos. Sci.,* **27,** 168–170.

Masunaga, H., and C. D. Kummerow, 2006: Observations of tropical precipitating clouds ranging from shallow to deep convective systems. *J. Geophys. Res.,* **33,** L16805, doi:10.1029/2006GL026547.

Meyers, M. P., P. J. Demott, and W. R. Cotton, 1992: New primary ice nucleation parameterizations in an explicit cloud model. *J. Appl. Meteor.,* **31,** 708–721.

Mohler, O., and Coauthors, 2005: Effect of sulfuric acid coating on heterogeneous ice nucleation by soot aerosol particles. *J. Geophys. Res.,* **110,** D11210, doi:10.1029/2004JD005169.

——, P. J. DeMott, G. Vali, and Z. Levin, 2007: Microbiology and atmospheric processes: The role of biological particles in cloud physics. *Biogeosciences,* **4,** 1059–1071.

Morris, C. E., D. C. Sands, M. Bardin, R. Jaenicke, B. Vogel, C. Leyronas, P. A. Ariya, and R. Psenner, 2011: Microbiology and atmospheric processes: Research challenges concerning the impact of airborne micro-organisms on the atmosphere and climate. *Biogeosciences,* **8,** 17–25.

Mossop, S. C., 1968: Comparison between concentration of ice crystals in cloud and the concentration of ice nuclei. *J. Rech. Atmos.,* **3,** 119–124.

——, 1976: Production of secondary ice particles during the growth of graupel by riming. *Quart. J. Roy. Meteor. Soc.,* **102,** 45–57.

——, 1978a: Some factors governing ice particle multiplication in cumulus clouds. *J. Atmos. Sci.,* **35,** 2033–2037.

——, 1978b: The influence of drop size distribution on the production of secondary ice particles during graupel growth. *Quart. J. Roy. Meteor. Soc.,* **104,** 323–330.

——, 1985: The origin and concentration of ice crystals in clouds. *Bull. Amer. Meteor. Soc.,* **66,** 264–273.

——, and E. R. Wishart, 1978: The mechanism of splintering during rime growth. *Geophys. Res. Lett.,* **5,** 1083–1085.

O'Dowd, C. D., M. H. Smith, I. E. Consterdine, and J. A. Lowe, 1997: Marine aerosol, sea-salt, and the marine sulphur cycle: A short review. *Atmos. Environ.,* **37,** 73–80.

Phillips, V. T. J., P. J. DeMott, and C. Andronache, 2008: An empirical parameterization of heterogeneous ice nucleation for multiple chemical species of aerosol. *J. Atmos. Sci.,* **65,** 2757–2783.

——, and Coauthors, 2009: Potential impacts from biological aerosols on ensembles of continental clouds simulated numerically. *Biogeosciences,* **6,** 987–1014.

Pratt, K. A., and Coauthors, 2009: *In situ* detection of biological particles in cloud ice-crystals. *Nat. Geosci.,* **2,** 398–401.

——, and Coauthors, 2010: In situ chemical characterization of aged biomass-burning aerosols impacting cloud wave clouds. *J. Atmos. Sci.,* **67,** 2451–2468.

Prenni, A. J., and Coauthors, 2009: Relative roles of biogenic emissions and Saharan dust as ice nuclei in the Amazon basin. *Nat. Geosci.,* **2,** 402–405.

Pruppacher, H. R., and J. D. Klett, 1997: *Microphysics of Clouds and Precipitation.* 2nd ed. Kluwer Academic Publishers, 954 pp.

Qian, Y., K. Willeke, V. Ulevicius, S. A. Grinshpun, and J. Donnelly, 1995: Dynamic size spectrometry of airborne microorganisms: Laboratory evaluation and calibration. *Atmos. Environ.,* **29,** 1123–1129.

Rangno, A. L., and P. V. Hobbs, 1991: Ice particle concentrations and precipitation development in small polar maritime cumuliform clouds. *Quart. J. Roy. Meteor. Soc.,* **117,** 207–241.

——, and ——, 2005: Microstructures and precipitation development in cumulus and small cumulonimbus clouds over the warm pool of the tropical Pacific Ocean. *Quart. J. Roy. Meteor. Soc.,* **131,** 639–673.

Richardson, M., and Coauthors, 2007: Measurements of heterogeneous ice nuclei in the western United States in springtime and their relation to aerosol characteristics. *J. Geophys. Res.,* **112,** D02209, doi:10.1029/2006JD007500.

Rodts, S. M. A., P. G. Duynkerke, and H. J. J. Jonker, 2003: Size distributions and dynamical properties of shallow cumulus clouds from aircraft observations and satellite data. *J. Atmos. Sci.,* **60,** 1895–1912.

Romps, D. M., and Z. Kuang, 2010: Do undiluted convective plumes exist in the upper tropical troposphere? *J. Atmos. Sci.,* **67,** 468–484.

Schär, C., and P. K. Smolarkiewicz, 1996: A synchronous and iterative flux-correction formalism for coupled transport equations. *J. Comput. Phys.,* **128,** 101–120.

Schlesinger, R. E., 1980: A three-dimensional numerical model of an isolated thunderstorm. Part II: Dynamics of updraft splitting and mesovortex couplet evolution. *J. Atmos. Sci.,* **37,** 395–420.

Sesartic, A., U. Lohmann, and T. Storelvmo, 2011: Bacteria in the ECHAM5-HAM global climate model. *Atmos. Chem. Phys. Discuss.,* **11,** 1457–1488.

Smolarkiewicz, P. K., and W. W. Grabowski, 1990: The multidimensional positive definite advection transport algorithm: Nonoscillatory option. *J. Comput. Phys.,* **86,** 355–375.

Sun, J., 2008: Ice initiation and ice multiplication processes in a warm-based precipitating cumulus cloud model. Ph.D. thesis, McGill University, 221 pp. [Available online at http://digitool. library.mcgill.ca/R/D2GKK6X24IDAR95I1B2JFJNRTFYFS 4E6HKUUNSVEV2MI1GMDVH-01083?func=results-jump-full&set_entry=000005&set_number=001334&base=GEN01-MCG02.]

——, and P. A. Ariya, 2006: Atmospheric organic and bio-aerosols as cloud condensation nuclei (CCN): A review. *Atmos. Environ.,* **40,** 795–820.

——, ——, H. G. Leighton, and M. K. Yau, 2010: Mystery of ice multiplication in warm-based precipitating shallow cumulus clouds. *Geophys. Res. Lett.,* **37,** L10802, doi:10.1029/2010GL042440.

Szyrmer, W., and I. Zawadzki, 1997: Biogenic and anthropogenic sources of ice-forming nuclei: A review. *Bull. Amer. Meteor. Soc.,* **78,** 209–228.

Tao, W.-K., X. Li, A. Khain, T. Matsui, S. Lang, and J. Simpson, 2007: Role of atmospheric aerosol concentration on deep convective precipitation: Cloud-resolving model simulations. *J. Geophys. Res.,* **112,** D24S18, doi:10.1029/2007JD008728.

Taylor, G. R., 1989: Sulfate production and deposition in midlatitude continental cumulus clouds. Part I: Cloud model formulation and base run analysis. *J. Atmos. Sci.,* **46,** 1971–1990.

Teller, A., and Z. Levin, 2006: The effects of aerosols on precipitation and dimensions of subtropical clouds: A sensitivity study using a numerical cloud model. *Atmos. Chem. Phys.,* **6,** 67–80.

Tong, Y., and B. Lightart, 2000: The annual bacterial particle concentration and size distribution in the ambient atmosphere in a rural area of the Willamette Valley, Oregon. *Aerosol Sci. Technol.,* **32,** 393–403.

Vali, G., M. Christensen, R. W. Fresh, E. L. Galyan, L. R. Maki, and R. C. Schnell, 1976: Biogenic ice nuclei. Part II: Bacteria sources. *J. Atmos. Sci.,* **33,** 1565–1570.

van den Heever, S. C., G. G. Carrio, W. R. Cotton, P. J. DeMott, and A. J. Prenni, 2006: Impacts of nucleating aerosol on Florida storms. Part I: Mesoscale simulations. *J. Atmos. Sci.,* **63,** 1752–1775.

Warren, S. G., R. M. Eastman, and C. J. Hahn, 2007: A survey of changes in cloud cover and cloud types over land from surface observations, 1971–96. *J. Climate,* **20,** 717–738.

Welti, A., F. Luond, O. Stetzer, and U. Lohmann, 2009: Influence of particle size on the ice nucleating ability of mineral dusts. *Atmos. Chem. Phys.,* **9,** 6705–6715.

Yau, M. K., 1979: Perturbation pressure and cumulus convection. *J. Atmos. Sci.,* **36,** 690–694.

——, 1980: A two-cylinder model of cumulus cells and its application in computing cumulus transports. *J. Atmos. Sci.,* **37,** 2470–2485.

Zhang, Y., and G. R. Carmichael, 1999: The role of mineral aerosol in tropospheric chemistry in East Asia—A model study. *J. App. Meteor.,* **38,** 353–366.

Zhao, M., and P. H. Austin, 2005: Life cycle of numerically simulated shallow cumulus clouds. *J. Atmos. Sci.,* **62,** 1291–1310.